Institute of Space and Aeronautical Science, University of Tokyo
Report No. 540, May 1976

On the Dynamic Stress Concentration of Notched Plates as Induced by Tensile Stress Waves

By

Kunihiko KUROKAWA and Koozo KAWATA

Summary: The dynamic stress concentration of notched plates as induced by tensile stress waves was analyzed numerically using the finite element method, and experimentally using the high-speed photo-elastic technique. The results were then compared with the approximate solution newly derived by the one-dimensional theory of stress wave propagation, and the effectiveness of this approximate solution of the dynamic stress concentration was confirmed.

§ 1. INTRODUCTION

Materials behave in very different manners when they are loaded statically and dynamically. When they are loaded dynamically the inertia must be taken into account, and deformations are propagated in the form of waves. In order to analyze the stress distributions of suddenly loaded material elements, wave equations must be solved. As for such problems as these, lots of one dimensional problems have been treated and solved in many cases, not only in elastic cases but also in non-elastic cases, but the treatment of examples of two or three dimensional problems have been restricted to simple boundary problems, and complex boundary problems have not yet been treated very much.

In this report the dynamic stress concentrations of notched plates (Fig. 1-1) as induced by tensile stress waves are analyzed. Up to the present this problem has been treated by K. Kawata and S. Hashimoto [*1, 2, 3*], and was analyzed using the one-dimensional theory and using a photo-elastic method with polyurethane rubber. In this paper, this problem is analyzed in the following three manners. The first is an approximate analysis using the one-dimensional theory of stress wave propagation, the second is a two-dimensional numerical analysis using the finite element method, and the last

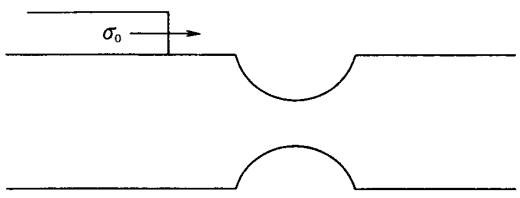

FIG. 1-1. Analyzed model.

This document is provided by JAXA.

is an experimental analysis using the technique of high-speed photo-elasticity.

In § 2 the one dimensional theory of stress wave propagation and its application to the problems of dynamic stress concentration are explained, and the approximate solution of the dynamic elastic stress concentration of notched plates as induced by stress waves is obtained.

In § 3 the applications of the finite element method to the dynamic problems are discussed. First, the one-dimensional problems are solved and compared with the analytical solution, and then extended to the two dimensional problems. Using this method the dynamic stress concentrations of notched plates as induced by stress waves are solved two dimensionally, and then the results are compared with the results of the approximate solution obtained in § 2. It is shown that the one-dimensional approximate solution gives a little higher value than two-dimensional numerical solution.

In § 4 the instruments and procedure for the experiment of high-speed photo-elasticity are explained. The experiment was performed using epoxy plate specimens. Then the results were compared with both the one-dimensional approximate solution and the numerical results of the finite element method.

In § 5 the conclusions are stated. The approximate solutions of dynamic stress concentration using the one-dimensional theory of stress wave propagation were confirmed as useful enough for engineering design by the use of two-dimensional numerical analysis and experimental analysis.

§ 2. The Approximate Solution by the One-Dimensional Theory

The elastic stress concentration of notched plates as induced by tensile stress waves can be considered to consist of two parts: the first resulting from differences in the cross-sectional areas, and the second from the stress gradient in the narrowest cross-section. In this approximate solution, the stress at the narrowest cross section obtained by the one-dimensional theory of elastic stress propagation is used for the first part, and for the second the elastic stress concentration factor for the statical case is used. In this chapter the one-dimensional theory of elastic stress propagation is stated in detail, and then the application of this theory to dynamic stress concentration is explained and an approximate solution is obtained.

2-1 Stress wave propagation in a one-dimensional media

Stress wave propagation in slender rods in which the inertia in the perpendicular direction of the axis can be neglected or in thick rods whose displacements in the perpendicular direction of the axis are perfectly restricted, will be described assuming that the cross-section of the rods is always kept in a vertical plane, and that the displacements of the particles of the same cross-section in the horizontal direction of the rod are kept equal (4).

Consider the infinitesimal element PQ of the length δx in a rod with a uniform cross-sectional area A (Fig. 2-1), where the x-axis is taken in ac-

This document is provided by JAXA.

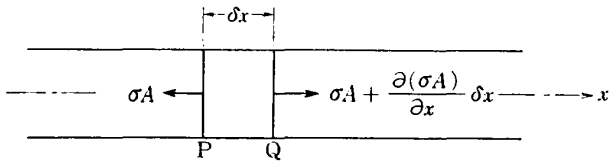

FIG. 2-1. Resultant stress components acting on an infinitesimal element of bar.

cordance with the axis of the rod. Let the stress which acts on section P be σ. Then the force which acts on this section will be σA, and that which acts on the section Q will be $\sigma A+\frac{\partial(\sigma A)}{\partial x}\delta x$. By Newton's second law of motion, neglecting body forces such as gravity, we have,

$$\rho A\delta x\frac{\partial^2 u}{\partial t^2}=\frac{\partial(\sigma A)}{\partial x}\delta x,$$

where ρ and u are the density and the displacement of the element respectively, and then,

$$\rho\frac{\partial^2 u}{\partial t^2}=\frac{\partial\sigma}{\partial x}. \tag{2-1}$$

Assuming Hooke's law between the stress σ and the strain $\varepsilon=\frac{\partial u}{\partial x}$, we have,

$$\sigma=k\frac{\partial u}{\partial x}, \tag{2-2}$$

where k is the elastic constant which varies according to the configuration of the rod. If the rod is slim and the inertia in the perpendicular direction of the axis may be neglected, this becomes,

$$k=E, \tag{2-2-a}$$

and if the rod is thick and particle displacements in the perpendicular direction of the axis may be considered to be restricted, the problem becomes a plane strain problem and k can be written as,

$$k=\frac{(1-\nu)E}{(1+\nu)(1-2\nu)}. \tag{2-2-b}$$

If the rod can be considered to be a thin plate, where the displacement of particles in one perpendicular direction of the axis is considered restricted, and where in another perpendicular direction the inertia is neglected, this problem becomes a plane stress problem and k can be written as,

$$k=\frac{E}{(1+\nu)(1-\nu)}. \tag{2-2-c}$$

In these equations, E and ν denote the Young's modulus and the Poisson's

This document is provided by JAXA.

ratio of the material respectively.

From Eqs. (2-1) and (2-2), we have the wave equation,

$$\rho\frac{\partial^2 u}{\partial t^2}=k\frac{\partial^2 u}{\partial x^2}. \tag{2-3}$$

The general solution of the wave equation, Eq. (2-3) can be written,

$$u=f(ct-x)+F(ct+x), \tag{2-4}$$

where

$$c=\sqrt{\frac{k}{\rho}}, \tag{2-5}$$

is the wave velocity. f and F of Eq. (2-4) are arbitrary functions of $(ct-x)$ and $(ct+x)$ respectively, and these denote the waves which propagate with the velocity c in the direction of increasing x and decreasing x. These must also always satisfy the given initial and boundary conditions.

Next we consider the wave which propagates only in the positive direction of x, so that Eq. (2-4) can be rewritten as,

$$u=f(ct-x). \tag{2-6}$$

Differentiating both sides of Eq. (2-6) in respect to x, we get,

$$\frac{\partial u}{\partial x}=-f'(ct-x), \tag{2-7}$$

where f' denotes the differentiation of the function f in respect to $(ct-x)$, and differentiating Eq. (2-6) in respect to t in the same manner, we get,

$$\frac{\partial u}{\partial t}=cf'(ct-x). \tag{2-8}$$

So that, from Eqs. (2-7) and (2-8),

$$\frac{\partial u}{\partial t}=-c\frac{\partial u}{\partial x}, \tag{2-9}$$

and then substituting into Eq. (2-2), we get the following relation,

$$\sigma=-\rho c\frac{\partial u}{\partial t}. \tag{2-10}$$

Eq. (2-10) denotes that there is a proportional relationship between the stress and the particle velocity at every point and that the proportional constant is $-\rho c$ for the wave propagating in the positive x direction. This shows that if the semi-infinite bar $x\geqq 0$ is pulled with a constant velocity V_0 at $x=0$ from $t=0$, the stress wave $\sigma_0=\rho c V_0$ will travel in the bar with a velocity c.

This document is provided by JAXA.

2-2 Stress elevation at the neck of the cross-section

In this section, we consider the case when the stress wave reaches a discontinuity in the cross section of the strip, and then induces stress elevation at the neck of the cross-sectional area. In practice, at the area of discontinuity of the cross-section complex reflections of waves are induced by the free boundaries, so that two (to be precise, three) dimensional analysis is needed. But here, in order to obtain the approximate solution we made our analysis on the assumption of the one-dimensional theory, in which the cross-sections which are perpendicular to the rod axis are kept plane and the displacements of the particles in the direction of the axis are always kept equal for the same cross section.

When the incident stress wave σ_I, which is travelling in material 1 from the negative x to the positive x direction, reaches the point of discontinuity between materials 1 and 2, O in Fig. 2-2, then the reflected wave σ_R is reflected into material 1 and the transmitted wave σ_T is transmitted into material 2. We choose the coordinate $x=0$ to coincide with O, and if we write the displacement in material 1 as induced by the incident wave from the negative x direction u_I, then

$$u_I=f_I(c_1t-x)\,, \tag{2-11}$$

and the stress σ_I becomes, as a result of the Eqs. (2-2) and (2-5),

$$\sigma_I=k_1\frac{\partial u_I}{\partial x}=-\rho c_1{}^2 f_I(c_1t-x)\,. \tag{2-12}$$

When this stress wave reaches the point of discontinuity, two types of stress waves are generated: they are the reflected stress wave σ_R in material 1 and the transmitted stress wave σ_T in material 2. If we write the displacement in material 1 induced by the reflected wave u_R and the displacement in material 2 induced by the transmitted wave u_T, they become,

$$u_R=F_R(c_1t+x)\,, \tag{2-13}$$

$$u_T=f_T(c_2t-x)\,, \tag{2-14}$$

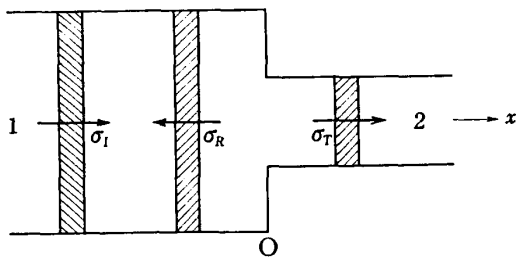

FIG. 2-2. Reflection and transmissin of stress wave at a discontinuity. When the incident stress wave σ_I reaches a discontinuity of the material, the reflected wave σ_R is reflected and the transmitted wave σ_T is transmitted.

This document is provided by JAXA.

and then by Eqs. (2-2) and (2-5) the induced stresses σ_R and σ_T become,

$$\sigma_R = k_1 \frac{\partial u_R}{\partial x} = \rho_1 c_1^2 F_R'(c_1 t + x), \tag{2-15}$$

$$\sigma_T = k_2 \frac{\partial u_T}{\partial x} = -\rho_2 c_2^2 f_T'(c_2 t - x). \tag{2-16}$$

The displacement and the stress in material 1 are produced by two types of waves, the incident wave and the reflected wave, and those in material 2 are produced by only one type of wave, the transmitted wave. By the principle of superposition the displacements and the stresses in materials 1 and 2 become as follows:

$$u_1 = u_I + u_R = f_I(c_1 t - x) + F_R(c_1 t + x), \tag{2-17}$$

$$u_2 = u_T = f_T(c_2 t - x), \tag{2-18}$$

$$\sigma_1 = \sigma_I + \sigma_R = \rho_1 c_1^2 \{-f_I'(c_1 t - x) + F_R'(c_1 t + x)\}, \tag{2-19}$$

$$\sigma_2 = \sigma_T = -\rho_2 c_2^2 f_T'(c_2 t - x). \tag{2-20}$$

The conditions of the continuity of displacement and the equilibrium of the force at the point of the discontinuity are,

$$u_1 = u_2 \qquad \text{at} \quad x = 0, \tag{2-21}$$

and,

$$A_1 \sigma_1 = A_2 \sigma_2 \qquad \text{at} \quad x = 0. \tag{2-22}$$

Substituting Eqs. (2-17) and (2-18) into Eq. (2-21), and Eqs. (2-19) and (2-20) into Eq. (2-22) we get,

$$f_I(c_1 t) + F_R(c_1 t) = f_T(c_2 t), \tag{2-23}$$

$$\rho_1 c_1^2 A_1 \{-f_I'(c_1 t) + F_R'(c_1 t)\} = -\rho_2 c_2^2 A_2 f_T'(c_2 t). \tag{2-24}$$

Differentiating Eq. (2-23) in respect to t,

$$c_1 \{f_I'(c_1 t) + F_R'(c_1 t)\} = c_2 f_T'(c_2 t). \tag{2-25}$$

At last, from Eqs. (2-12), (2-15), (2-16), (2-24) and (2-25), the magnitude of the reflected and the transmitted stress waves can be represented using the magnitude of the incident stress wave as follows:

$$\sigma_R = \frac{\rho_2 c_2 A_2 - \rho_1 c_1 A_1}{\rho_1 c_1 A_1 + \rho_2 c_2 A_2} \sigma_I, \tag{2-26}$$

$$\sigma_T = \frac{2\rho_2 c_2 A_1}{\rho_1 c_1 A_1 + \rho_2 c_2 A_2} \sigma_I. \tag{2-27}$$

When materials 1 and 2 are the same, and when only the cross sectional areas between 1 and 2 are different, then the Eqs. (2-26) and (2-27) become

This document is provided by JAXA.

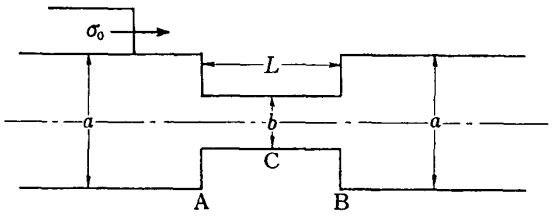

FIG. 2-3. The model of a strip with a neck.

simpler as follows:

$$\sigma_R=\frac{A_1-A_2}{A_1+A_2}\sigma_I\,, \tag{2-28}$$

$$\sigma_T=\frac{2A_1}{A_1+A_2}\sigma_I\,. \tag{2-29}$$

Next, using this theory we considered the stress elevation at the neck of the cross-sectional area in the strip shown in Eig. 2-3. When the stepped stress wave σ_0 reaches A from the left side, transmitted and reflected waves are produced, and their magnitudes are given by Eqs. (2-28) and (2-29). When the transmitted stress wave reaches B, some of it is reflected into A. Then, the reflected wave produces other reflected waves one another at A and B. At the end the stress σ_1 at C is given by the following equations,

$$\left.\begin{array}{ll}
t-t_0<0; & \sigma_1=0 \\
0<t-t_0<\dfrac{L}{c}; & \sigma_1=\sigma_T=\dfrac{2a}{a+b}\sigma_0 \\
\dfrac{L}{c}<t-t_0<\dfrac{2L}{c}; & \sigma_1=\left\{1+\dfrac{a-b}{a+b}\right\}\sigma_T \\
\dfrac{2L}{c}<t-t_0<\dfrac{3L}{c}; & \sigma_1=\left\{1+\dfrac{a-b}{a+b}+\left(\dfrac{a-b}{a+b}\right)^2\right\}\sigma_T \\
\quad\vdots & \quad\vdots \\
\dfrac{nL}{c}<t-t_0<\dfrac{(n+1)L}{c}; & \sigma_1=\left\{1-\dfrac{a-b}{a+b}+\left(\dfrac{a-b}{a+b}\right)^2+\cdots+\left(\dfrac{a-b}{a+b}\right)^n\right\}\sigma_T \\
\quad\vdots & \quad\vdots \\
t\to\infty; & \sigma_1=\dfrac{a}{b}\sigma_0
\end{array}\right\} \tag{2-30-a}$$

where t_0 is the time when the first wave front reaches C. This result is shown in Eig. 2-4. Connecting the peak points of step function, σ_1 is approximated as follows:

$$\sigma_1=\frac{1-\left(\dfrac{a-b}{a+b}\right)^{\frac{c(t-t_0)}{L}+1}}{1+\dfrac{a-b}{a+b}}\sigma_0=\left\{1-\left(\frac{a-b}{a+b}\right)^{\tau+1}\right\}\frac{a}{b}\sigma_0\,, \tag{2-30-b}$$

This document is provided by JAXA.

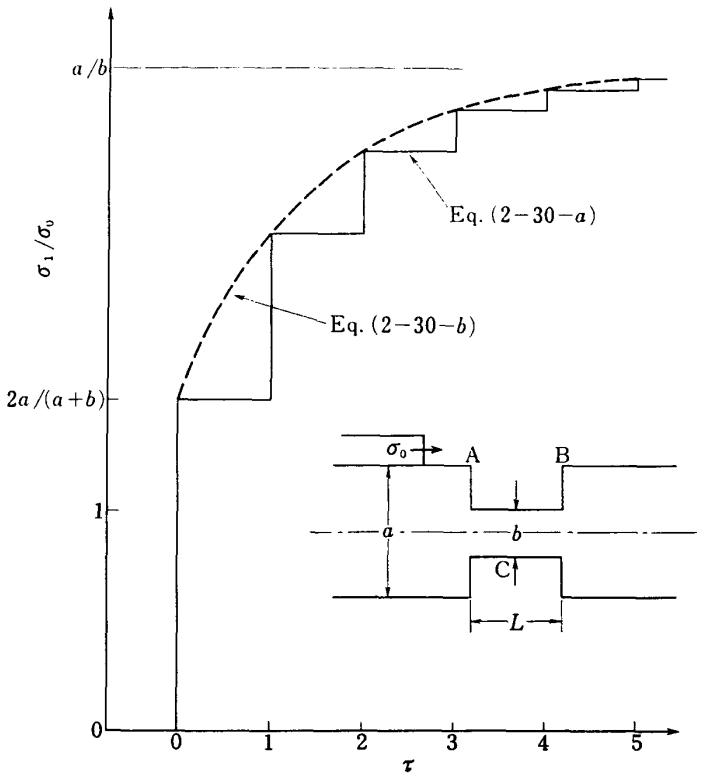

FIG. 2-4. The stress change at the middle point of the neck. The full line denote Eq. (2-30-a), and dotted line Eq. (2-30-b).

where,

$$\tau=\frac{c(t-t_0)}{L}.$$

2-3 Approximate solution of the dynamic stress concentration

In this section we will derive the approximate solution of the dynamic stress concentration at the bottom of the notch, E of Fig. 2-5, as induced by the stress waves. First, we considered the case when the incident stress wave is given by a step function with the magnitude σ_0, and then we extended it to the arbitrary type of incident stress wave.

We can consider two factors which cause dynamic stress concentration at the bottom of the notch in a strip. The first factor depends on the configuration of the notch, and results from the stress gradient in the narrowest cross section. For this factor we use the coefficient for the statical case, that is, the statical stress concentration factor α, and this value can be obtained experimentally or numerically. Especially for the shapes which were adopted for our analysis, we may use the experimental data (5),

$$\alpha=1+\left\{\frac{1}{1.55\frac{a}{b}-1.3}\frac{d}{r}\right\}^n, \tag{2-31}$$

where,

This document is provided by JAXA.

$$n=\frac{\left(\frac{a}{b}-1\right)+0.5\sqrt{\frac{d}{r}}}{\left(\frac{a}{b}-1\right)+\sqrt{\frac{d}{r}}}.$$

The second factor depends on the dynamic behavior caused by the variation of the cross-sectional area, and for this factor we use the approximate solution derived by the one-dimensional theory, which was stated in last section. To begin with, we approximated the arc A′ED′ by the straight lines ABECD, where AB(DC) is selected so that the crossing point of AB(DC) and the arc A′E(D′E) becomes the middle point of A(D) and B(C). In other, previous works (1, 2, 3), A and D were so selected as to coincide with A′ and D′ respectively, as shown in Fig. 2-6, so that L was equal to the

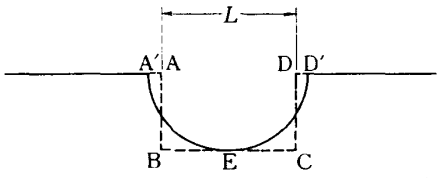

FIG. 2-5. The approximation of curved boundary by straight lines.

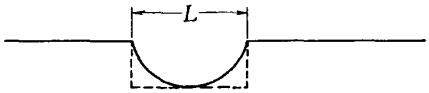

FIG. 2-6. The approximation of curved boundary which was used in the preceding analyses (1, 2, 3).

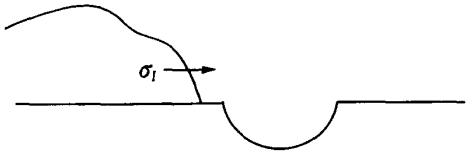

FIG. 2-7. The dynamic stress concentration by the stress wave with arbitrary shape.

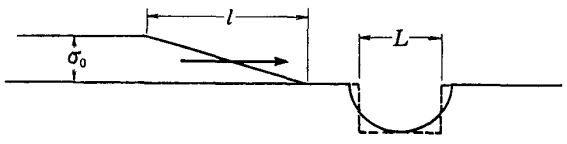

FIG. 2-8. The Simpler form of the incident stress wave.

This document is provided by JAXA.

whole length of the notch. To the shape ABECD, we applied the one dimensional theory, and obtained the stress elevating factor which depends on the cross-sectional area. This factor is represented by σ_1 in Eqs. (2-30).

In conclusion, the approximate solution of the stress at E in Fig. 2-5 can be written as,

$$\sigma=\alpha\sigma_1\,, \tag{2-32}$$

where α is the statical elastic stress concentration factor and σ is the stress obtained by the one-dimensional theory of elastic stress propagation and given by Eqs. (2-30).

Next, we extend this approximate solution to the case when the incident stress wave $\sigma_I(t')$ ($\sigma_I(t')=0$ for $t'<0$) has an arbitrary shape as shown in Fig. 2-7. Using the relations of Eqs. (2-30), where the incident stress wave is given by σ_I, the stress σ_1 becomes as follows:

$$\sigma_1=\begin{cases}0 & (\text{for } t<t_0)\\ \displaystyle\int_0^{t-t_0}\phi(t-t_0-t')\frac{a}{b}\frac{\partial\sigma_I(t')}{\partial t'}dt' & (\text{for } t\geqq t_0)\,,\end{cases} \tag{2-33}$$

where t_0 is the time when the wave front reaches the bottom of the notch, and $\phi(t)$ is a function which is obtained from Eq. (2-30-a) as follows:

$$\phi_{(t)}=\begin{cases}0 & (\text{for } t<0)\\ 1-\left(\dfrac{a-b}{a+b}\right)^{n+1} & (\text{for } nL\leqq ct\leqq(n+1)L)\,,\end{cases} \tag{2-34-a}$$

or, as an approximate form of Eq. (2-30-b),

$$\phi_{(t)}=\begin{cases}0 & (\text{for } t<0)\\ 1-\left(\dfrac{a-b}{a+b}\right)^{\frac{c}{L}t+1} & (\text{for } t\geqq 0)\,.\end{cases} \tag{2-34-b}$$

When the incedent stress wave σ_I is simple as in Fig. 2-8, $\partial\sigma_I/\partial t$ is represented as,

$$\frac{\partial\sigma_I}{\partial t'}=\frac{\partial\sigma_I}{\partial x}\frac{\partial x}{\partial t'}=\begin{cases}0 & (\text{for } t<0)\\ \dfrac{c}{l}\sigma_0 & \left(\text{for } 0\leqq t\leqq\dfrac{l}{c}\right)\\ 0 & \left(\text{for } t>\dfrac{l}{c}\right)\end{cases} \tag{2-35}$$

so that σ_1 given by Eq. (2-33) becomes as follows:

$$\sigma_1(\tau)=\begin{cases}0 & (\text{for } \tau<0)\\ \left\{\tau+\dfrac{m}{ln(m)}(1-m^{\tau})\right\}\dfrac{L}{l}\dfrac{a}{b}\sigma_0 & \left(\text{for } 0\leqq\tau\leqq\dfrac{l}{L}\right)\\ \left\{1+\dfrac{L}{l}\dfrac{m^{\tau+1}}{ln(m)}(m^{-l/L}-1)\right\}\dfrac{a}{b}\sigma_0 & \left(\text{for } \tau\geqq\dfrac{l}{L}\right),\end{cases} \tag{2-36}$$

This document is provided by JAXA.

where τ and m are

$$\tau=\frac{(t-t_0)c}{L}, \qquad m=\frac{a-b}{a+b},$$

and where for the function ϕ, the approximate Eq. (2-34-b) is used.

§ 3. Two Dimensional Analysis Using the Finite Element Method

In this chapter, dynamic stress concentration is analyzed numerically using the finite element method, and the results are compared with the one-dimensional approximate solution.

3-1 Application of the finite element method to the dynamic elasticity

The outline of the finite element method used for this analysis, in which the displacement method is used, is described in this section. The details of this method can be found in other books concerning this method (6, 7), so that only the outlines are stated here.

This method can be considered in the following manner;

1) The continuum is separated into a number of 'finite elements' by imaginary lines or surfaces.

2) The elements are assumed to be interconnected at a discrete number of nodal points situated on their boundaries. The displacements of these nodal points are the basic unknown parameters of the problem.

3) A function (or functions) is chosen to define uniquely the state of displacement within each 'finite element' in terms of its nodal displacements. Here, the displacement must be so defined as to be kept continuous through the imaginary lines or surfaces.

4) The displacement functions now define uniquely the state of strain within an element in terms of the nodal displacements. Then, the virtual displacements at each nodal point are considered. The virtual work done by external forces and virtual displacements is equal to the internal work produced by the virtual displacements. So that simultaneous equations can be obtained, and the inertia, here, is taken into account in the form of distributed forces using the d'Alembert's principle.

5) The displacements of the nodal points are obtained by solving the above simultaneous equations, and then, the strains and stresses are obtained.

Next, formulating the method by the above manner, we can define the displacement in a 'finite element' in the continuum by the displacements of the nodal points representing the element. If we denote the displacement in the elements $\{\boldsymbol{f}\}$ and displacements of the nodal points $\{\delta\}^e$, we can write,

$$\{\boldsymbol{f}\}=[\boldsymbol{N}]\{\delta\}^e, \tag{3-1}$$

where $[\boldsymbol{N}]$ is the matrix connecting $\{\boldsymbol{f}\}$ and $\{\delta\}^e$. The matrix $[\boldsymbol{N}]$ must be so defined so that the continuity of the displacements can be kept through

This document is provided by JAXA.

the boundary of the elements. The relation between the displacement within the element and the displacements of the nodal points is defined, so that the relation between the strain $\{\varepsilon\}$ and the displacements of the nodal points can be defined as,

$$\{\varepsilon\} = [\boldsymbol{B}][\delta]^e, \tag{3-2}$$

where $[\boldsymbol{B}]$ is the matrix connecting $\{\varepsilon\}$ and $\{\delta\}^e$, and can be defined using relation Eq. (3-1) and the strain-displacement relationships. The stress $\{\sigma\}$ can be written as,

$$\{\sigma\} = [\boldsymbol{D}]\{\varepsilon\}, \tag{3-3}$$

where $[\boldsymbol{D}]$ represents the stress-strain relationship of the material.

The actual applied loads are usually distributed, *e.g.*, by pressure loading, on structural elements, and the body forces and inertia are distributed through the elements. Therefore a technique is required for determining equivalent concentrated forces at the location and direction of the element forces. These equivalent forces can be obtained using the principle of virtual work.

Next, we consider virtual displacements $\{\delta^*\}^e$ at the nodal points, this is, the displacements $\{\delta\}^e$ are varied to $\{\delta\}^e + \{\delta^*\}^e$. Then the increments of the displacements and strains in the element produced by the virtual displacements at the nodal points can be written by Eqs. (3-1) and (3-2) as follows:

$$\{\boldsymbol{f}^*\} = [\boldsymbol{N}]\{\delta^*\}^e, \qquad \{\varepsilon^*\} = [\boldsymbol{B}]\{\delta^*\}^e. \tag{3-4}$$

The virtual work produced by the virtual displacements can be considered as the inner product of the equivalent concentrated forces at the nodal points $\{\boldsymbol{F}\}^e$ and the virtual displacements, so that,

$$(\{\delta^*\}^e)^T\{\boldsymbol{F}\}^e. \tag{3-5}$$

On the other hand, the increment of the internal energy of the stress and the distributed forces $\{\boldsymbol{p}\}$ can be written as,

$$\{\varepsilon^*\}^T\{\sigma\} - \{\boldsymbol{f}^*\}^T\{\boldsymbol{p}\}, \tag{3-6}$$

per unit volume. Substituting Eq. (3-4) into Eq. (3-6) we get,

$$(\{\delta^*\}^e)^T([\boldsymbol{B}]^T\{\sigma\} - [\boldsymbol{N}]^T\{\boldsymbol{p}\}). \tag{3-7}$$

The virtual work done by the equivalent concentrated forces is represented by Eq. (3-5), and the virtual work is equal to the total internal work given by the integral of Eq. (3-7) through the whole body, so that the relation,

$$(\{\delta^*\}^e)^T\{\boldsymbol{F}\}^e = (\{\delta^*\}^e)^T\left\{\int[\boldsymbol{B}]^T\{\sigma\}\,d(vol) - \int[\boldsymbol{N}]^T\{\boldsymbol{p}\}\,d(vol)\right\}, \tag{3-8}$$

is obtained. This relation is valid for any set of virtual displacements $\{\delta^*\}^e$, so that the equivalent concentrated forces can be written as,

This document is provided by JAXA.

$$\{F\}^e=\int[B]^T\{\sigma\}\,d(vol)-\int[N]^T\{p\}\,d(vol)\,. \tag{3-9}$$

For the case of dynamic problems, an incremental representation of the relation Eq. (3-9) is necessary. The incremental representation of Eq. (3-9) can be written as,

$$\{\Delta F\}^e=\int[B]^T\{\Delta\sigma\}\,d(vol)-\int[N]^T\{\Delta p\}\,d(vol)\,, \tag{3-10}$$

where $\{\Delta F\}^e$, $\{\Delta\sigma\}$, and $\{\Delta p\}$ are the increments of the equivalent concentrated forces, the stresses, and the distributed forces from time$=t$ to $t+\Delta t$ respectively. They represent $\{\Delta F\}_t=\{F\}_{t+\Delta t}{}^e-\{F\}_t{}^e$, $\{\Delta\sigma\}=\{\sigma\}_{t+\Delta t}-\{\sigma\}_t$, and $\{\Delta p\}=\{p\}_{t+\Delta t}-\{p\}_t$ respectively, and $\{F\}_t$, $\{\sigma\}_t$, and $\{p\}_t$ are respectively the equivalent concentrated forces, stresses, and distributed forces at t. The incremental representation of the stresses are obtained from Eqs. (3-2) and (3-3) as,

$$\{\Delta\sigma\}=[D]\{\Delta\varepsilon\}=[D][B]\{\Delta\delta\}^e\,. \tag{3-11}$$

If only the forces reduced by the inertia are taken into account as the distributed forces, the incremental representation of these forces becomes,

$$\{\Delta p\}=-\rho\{\Delta\ddot{f}\}=-\rho[N]\{\Delta\ddot{\delta}\}^e\,, \tag{3-12}$$

where ρ is the density and $\{\Delta\ddot{\delta}\}$ is the increments of the accelerations of the nodal points. Substituting Eqs. (3-11) and (3-12) into Eq. (3-10), the relation,

$$\{\Delta F\}^e=[k]^e\{\Delta\delta\}^e+[m]^e\{\Delta\ddot{\delta}\}^e\,, \tag{3-13}$$

is obtained, where $[k]^e$ and $[m]^e$ are the stiffness matrix and the mass matrix of the element respectively, and these can then be written as,

$$[k]^e=\int[B]^T[D][B]d(vol)\,,\quad [m]^e=\int\rho[N]^T[N]d(vol)\,. \tag{3-14}$$

Adding Eq. (3-13) for all elements, the 2nd order simultaneous differential equations

$$[M]\{\Delta\ddot{\delta}\}+[K]\{\Delta\delta\}=\{\Delta F\}\,, \tag{3-15}$$

are obtained, where $[M]$ and $[K]$, are the mass matrix and the stiffness matrix for all elements of this system respectively, and $\{\Delta\delta\}$ and $\{\Delta F\}$ are the vector representations of the increments of the displacements and equivalent concentrated forces for all the nodal points of this system respectively.

By using the incremental displacements of the nodal points instead of the incremental accelerations in Eq. (3-15), sinultaneous algebraic equations can be obtained instead of 2nd order simultaneous differential equations. Therefore the acceleration of the nodal point $\ddot{\delta}$ is assumed to vary linearly against

This document is provided by JAXA.

time t between the infinitesimal time, t to $t+\Delta t$. In this way the increments of the displacement, the velocity and the acceleration from time t to $t+\Delta t$ can be written respectively as,

$$\Delta\delta=\dot{\delta}_t\Delta t+\frac{1}{2}\ddot{\delta}_t\Delta t^2+\frac{1}{6}\dddot{\delta}_t\Delta t^3,$$

$$\Delta\dot{\delta}=\ddot{\delta}_t\Delta t+\frac{1}{2}\dddot{\delta}_t\Delta t^2,$$

$$\Delta\ddot{\delta}=\dddot{\delta}_t\Delta t.$$

In these equations, $\dot{\delta}_t$ and $\ddot{\delta}_t$ are known at t. Solving the above equations for $\Delta\dot{\delta}$ and $\Delta\ddot{\delta}$, we can get,

$$\Delta\dot{\delta}=\frac{3}{\Delta t}\Delta\delta-3\dot{\delta}_t-\frac{\Delta t}{2}\ddot{\delta}_t,\qquad \Delta\ddot{\delta}=\frac{6}{\Delta t^2}\Delta\delta-\frac{6}{\Delta t}\dot{\delta}_t-3\ddot{\delta}_t. \tag{3-16}$$

Substituting Eq. (3-16) into the equations (3-15), the 2nd order simultaneous differential equations can be rewritten by the simultaneous algebraic equations as follows,

$$\left([\boldsymbol{K}]+\frac{6}{\Delta t^2}[\boldsymbol{M}]\right)\{\Delta\delta\}=\{\Delta\boldsymbol{F}\}+[\boldsymbol{M}]\left(\frac{6}{\Delta t}\{\dot{\delta}\}_t+3\{\ddot{\delta}\}_t\right). \tag{3-17}$$

In conclusion, by solving the equations (3-17), the increments of the displacements $\{\Delta\delta\}$ can be obtained, and then substituting into the relations Eqs. (3-16), the increments of the velocities and the accelerations are obtained. Thus the new state of the displacements, velocities and the accelerations of the nodal points at time $t+\Delta t$ can be obtained from those at t, and by repeating this process, the dynamic problems can be solved.

3-1-1 Computer calculation flow

Computer calculation flow is as follows:

1) Data input; read the coordinates of the points, the components of the elements, the material constants, etc..

2) Formation of the stiffness and mass matrices, $[\boldsymbol{K}]$ and $[\boldsymbol{M}]$; the matrices for the whole system are formed from the stiffness matrix $[\boldsymbol{k}]^e$ and the mass matrix $[\boldsymbol{m}]^e$ of each element (Eq. (3-14)).

3) Initial conditions; give the initial condition, the velocities and the accelerations of the nodal points at $t=0$. (In this paper, the initial strain problems are not treated.)

4) Boundary conditions; the change of the boundary conditions, and the increments of the applied forces or the displacements, from $t=t$ to $t+\Delta t$ are given.

5) Formation of the right hand side of the equation (3-17); form the right hand side of the equation (3-17). Here, the terms $\{\dot{\delta}\}_t$, $\{\ddot{\delta}\}_t$ and $\{\Delta\boldsymbol{F}\}$ were given previously.

6) Solve the simultaneous equations (3-17); solve the simultaneous equa-

This document is provided by JAXA.

tions (3-17) using the conjugated gradient method, and then calculate the increment of the equivalent concentrated forces of the restricted nodal points.

7) Calculate the new state; using the increments of the displacements of the nodal points, the increments of the velocities and the accelerations of the nodal points are calculated (Eq. (3-16)), and the increments of the equivalent concentrated forces are added to the present condition.

8) Output of the result; print the results in accordance with the demand. The strains and stresses are obtained using Eqs. (3-2) and (3-3).

9) Repeat; go back to 4) and repeat.

3-1-2 Application to the one dimensional problem

In this section, one dimensional elastic stress wave propagation is solved numerically using the finite element method, and is compared with the analytical solution. Consider a small element of length l in a rod with the cross-sectional area A and the Young's modulus E (Fig. 3-1). Taking the x-axis in accordance with the axis of the rod, and the nodal points of both ends of the element to be i and j, we write the coordinates and the displacements of the points i and j as x_i, x_j, and δ_i, δ_j, respectively. Assuming that the displacement varies linearly in the element and using the small displacement theory, we can write,

$$\{\delta\}^e=\begin{Bmatrix}\delta_i\\ \delta_j\end{Bmatrix}, \quad \{\varepsilon\}=\varepsilon=\frac{\partial u}{\partial x}, \quad \{\sigma\}=\sigma, \tag{3-18}$$

where ε, σ and u are the strain, stress, and the displacement. Then the matrices defined by the relations Eqs. (3-1), (3-2) and (3-3) become,

$$[\boldsymbol{N}]=\left[\frac{x_i-x}{x_j-x_i}, \frac{x-x_i}{x_j-x_i}\right], \tag{3-19}$$

$$[\boldsymbol{B}]=\frac{1}{x_j-x_i}[-1, 1]=\frac{1}{l}[-1, 1], \tag{3-20}$$

$$[\boldsymbol{D}]=E. \tag{3-21}$$

This way, substituting Eqs. (3-19), (3-20), and (3-21) into Eq. (3-14), the stiffness matrix and the mass matrix of the element can be written as follows,

$$[\boldsymbol{k}]^e=\frac{AE}{l}\begin{bmatrix}1 & -1\\ -1 & 1\end{bmatrix}, \tag{3-22}$$

and,

$$[\boldsymbol{m}]^e=\rho Al\begin{bmatrix}\frac{1}{3} & \frac{1}{6}\\ \frac{1}{6} & \frac{1}{3}\end{bmatrix}. \tag{3-23}$$

Using the above mensioned method, a practical example is then solved. A rod (Fig. 3-2), whose sectional area A, density ρ, Young's modulus E, and

This document is provided by JAXA.

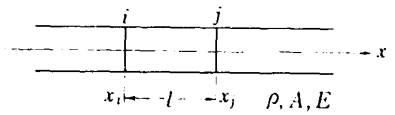

FIG. 3-1. An element of a continuum in one dimensional problem.

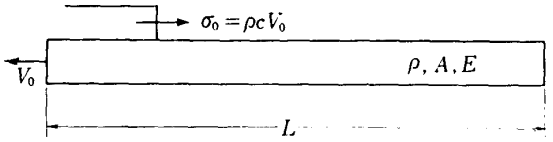

FIG. 3-2. The analyzed model. $\rho = 8 \times 10^{-10}$ kg-sec^2/mm^4, $A = 1$ mm^2, $E = 2 \times 10^4$ kg/mm^2, $L = 100$ mm, and was divided into 100 elements by 101 nodal points, $l = 1$ mm, $V_0 = 1 \times 10^4$ mm/sec, $c_0 = 5 \times 10^6$ mm/sec, $\sigma_0 = 40$ kg/mm^2.

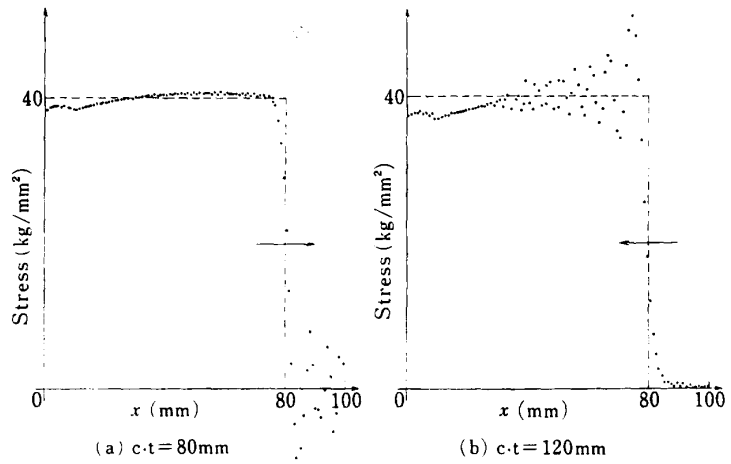

FIG. 3-3. The numerical results of the one-dimensional stress wave propagation by the finite element method. ($c \cdot \Delta t/l = 0.2$)

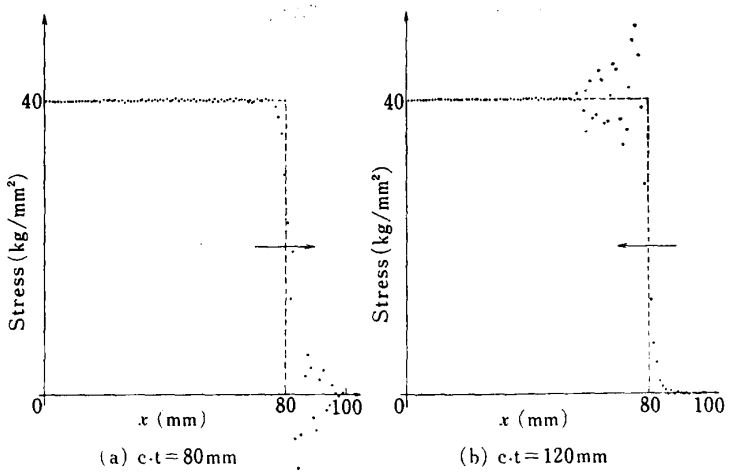

FIG. 3-4. The numerical results of the one-dimensional stress wave propagation by the finite element method. ($c \cdot \Delta t/l = 0.6$)

This document is provided by JAXA.

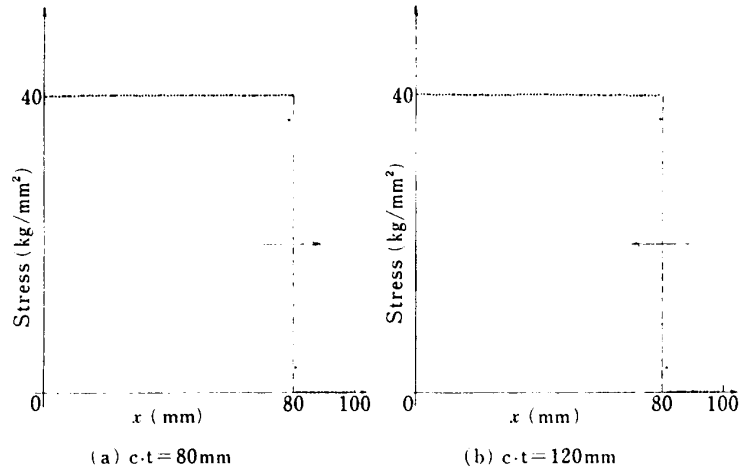

FIG. 3-5. The numerical results of the one-dimensional stress wave propagation by the finite element method. ($c \cdot \Delta t/l = 1.0$)

length L are 1 mm², 8×10^{-10} kg-sec²/mm⁴, 2×10^4 kg/mm² and 100 mm respectively, is divided equally into 100 elements, so that the length of a element l is 1 mm. When the left end of the rod is pulled with the constant velocity $V_0 = 1 \times 10^4$ mm/sec from $t=0$, then the elastic stress wave $\sigma_0 = -\rho c V_0 = 40$ kg/mm² travels to the right-hand direction with the wave velocity $c_0 = 5 \times 10^6$ mm/sec, and when the stress wave reaches the right end, a reflected wave is created and travels to the left direction. The total stress is zero at wherever the reflected wave front has reached. The numerical solutions of this phenomenon are shown in Figs. 3-3, 3-4, and 3-5. In the repeating calculation, a time increment Δt of one step was taken so as to be $c_0 \Delta t/l = 0.2$, 0.6, and 1.0, and the results when $c_0 t$ is 80 mm and 120 mm are shown. For all cases, the stresses behind the wave front shows close agreement with the analytical solution, but for the cases $c_0 \Delta t/l = 0.2$, and 0.6 the disturbances are spread in front of the stress front, especially for the case $c_0 \Delta t/l = 0.2$. The case $c_0 \Delta t/l = 1$ corresponds to the case when the calculations are done following wave equation characteristics, and the numerical solution agrees with the analytical solution. When $c_0 \Delta t/l$ is taken greater than 1, the solution diverged with the time. These results show that the numerical solution by the finite element method is sufficient enough for use in analyzing stress wave propagation.

3-1-3 Application to plane problems

In this section, the application of the finite element method to the problems of elastic stress propagation in isotropic and homogeneous materials in a plane state is treated. The only difference between the analyses of plane state is treated. The only difference between the analyses of plane stress, where the plate is so thin that the inertia in the direction of the thickness can be neglected and the stress component of this direction may be considered to be zero, and that of plane strain, where the plate is so thick that the displacement in the direction of the thickness may be considered to be

This document is provided by JAXA.

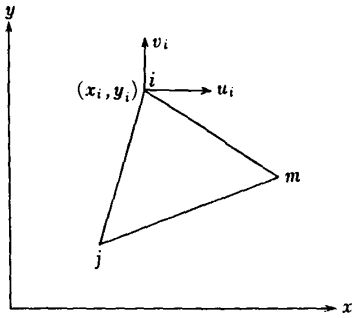

FIG. 3-6. An element of a continuum in plane stress or plane strain.

zero, is the difference of the stress-strain matrices.

Consider a triangular element i, j, m as shown in Fig. 3-6. In this system, the displacements consist of two components u and v, in the x and y directions respectively, and consequently the nodal point i has two components of displacement u_i and v_i. They can be written as,

$$\{\delta_i\} = \begin{Bmatrix} u_i \\ v_i \end{Bmatrix}, \tag{3-24}$$

and every component of the displacement of the three nodal points concerning this element can be written as follows:

$$\{\delta\}^e = \begin{Bmatrix} \{\delta_i\} \\ \{\delta_j\} \\ \{\delta_m\} \end{Bmatrix}. \tag{3-25}$$

The simplest way to uniquely represent the displacements u and v in this element using the six components of Eq. (3-25) is

$$\left.\begin{aligned} u &= \alpha_1 + \alpha_2 x + \alpha_3 y, \\ v &= \alpha_4 + \alpha_5 x + \alpha_6 y. \end{aligned}\right\} \tag{3-26}$$

The six constants α_i $(i=1\sim6)$ can be obtained by substituting the coordinates of each nodal point into Eq. (3-26) and u and v become,

$$\left.\begin{aligned} u &= \frac{1}{2\Delta}\{(a_i+b_i x+c_i y)u_i+(a_j+b_j x+c_j y)u_j+(a_m+b_m x+c_m y)u_m\}, \\ v &= \frac{1}{2\Delta}\{(a_i+b_i x+c_i y)v_i+(a_j+b_j x+c_j y)v_j+(a_m+b_m x+c_m y)v_m\}, \end{aligned}\right\} \tag{3-27}$$

where $a_i, \cdots, c_m$ respectively denote,

$$\left.\begin{aligned} a_i &= x_j y_m - x_m y_j, \\ b_i &= y_j - y_m = y_{jm}, \\ c_i &= x_m - x_j = x_{mj}. \end{aligned}\right\} \tag{3-28}$$

This document is provided by JAXA.

a_j, b_j, $\cdots$, and c_m can be obtained by a cyclic permutation of subscripts in the order i, j, m. Δ is,

$$2\Delta=\begin{vmatrix}1 & x_i & y_i\\ 1 & x_j & y_j\\ 1 & x_m & y_m\end{vmatrix}=2\times(\text{area of triabgle } ijm). \tag{3-29}$$

We can represent the above mentioned Eqs. (3-27) in the standard form of Eq. (3-1):

$$\{\boldsymbol{f}\}=\begin{Bmatrix}u\\ v\end{Bmatrix}=[\boldsymbol{I}N_i,\ \boldsymbol{I}N_j,\ \boldsymbol{I}N_m]\{\delta\}^e, \tag{3-30}$$

with $\boldsymbol{I}$ a two by two identity matrix, and

$$N_i=(a_i+b_ix+c_iy)/(2\Delta),\ \text{etc.}. \tag{3-31}$$

The chosen displacement function automatically guarantees the continuity of displacements with adjacent elements because the displacements vary linearly along each side of the triangle, and because of the identical displacement imposed at the nodes, the same displacements will clearly exist at all points along each interface.

The total strain at any point within the element which contributes to internal work can be defined by its three components, as

$$\{\varepsilon\}=\begin{Bmatrix}\varepsilon_x\\ \varepsilon_y\\ \varepsilon_{xy}\end{Bmatrix}=\begin{Bmatrix}\dfrac{\partial u}{\partial x}\\ \dfrac{\partial v}{\partial y}\\ \dfrac{\partial u}{\partial y}+\dfrac{\partial v}{\partial x}\end{Bmatrix}. \tag{3-32}$$

Using Eqs. (3-27) and (3-32), the $[\boldsymbol{B}]$ matrix of Eq. (3-2) becomes,

$$[\boldsymbol{B}]=\frac{1}{2\Delta}\begin{bmatrix}b_i & 0 & b_j & 0 & b_m & 0\\ 0 & c_i & 0 & c_j & 0 & c_m\\ c_i & b_i & c_j & b_j & c_m & b_m\end{bmatrix}. \tag{3-33}$$

It will be noted that in this case the $[\boldsymbol{B}]$ matrix is independent of position within the element, and hence the strains are constant throughout it.

The stress-strain matrix $[\boldsymbol{D}]$ is different for the cases of plane stress and plane strain. For the case of plane stress problems, the $[\boldsymbol{D}]$ matrix is,

$$[\boldsymbol{D}]=\frac{E}{1-\nu^2}\begin{bmatrix}1 & \nu & 0\\ \nu & 1 & 0\\ 0 & 0 & \dfrac{(1-\nu)}{2}\end{bmatrix}, \tag{3-34a}$$

and for the case of plane strain problems, the $[\boldsymbol{D}]$ matrix becomes,

This document is provided by JAXA.

$$[\boldsymbol{D}]=\frac{(1+\nu)(1-2\nu)}{(1-\nu)E}\begin{bmatrix} 1 & \frac{\nu}{(1-\nu)} & 0 \\ \frac{\nu}{(1-\nu)} & 1 & 0 \\ 0 & 0 & \frac{(1-2\nu)}{2(1-\nu)} \end{bmatrix}, \tag{3-34b}$$

where E and ν are the Young's modulus and the Poisson's ratio respectively.

From the general relationship Eq. (3-33), and Eq. (2-31) the stiffness matrix and the mass matrix of the element ijm are defined as,

$$[\boldsymbol{k}]^e=\int[\boldsymbol{B}]^T[\boldsymbol{D}][\boldsymbol{B}]d(vol)=[\boldsymbol{B}]^T[\boldsymbol{D}][\boldsymbol{B}]t\Delta, \tag{3-35}$$

and

$$[\boldsymbol{m}]^e=\int\rho[\boldsymbol{N}]^T[\boldsymbol{N}]d(vol)=\frac{\rho t\Delta}{12}\begin{bmatrix} 2 & 0 & 1 & 0 & 1 & 0 \\ 0 & 2 & 0 & 1 & 0 & 1 \\ 1 & 0 & 2 & 0 & 1 & 0 \\ 0 & 1 & 0 & 2 & 0 & 1 \\ 1 & 0 & 1 & 0 & 2 & 0 \\ 0 & 1 & 0 & 1 & 0 & 2 \end{bmatrix}, \tag{3-36}$$

where t is the thickness of the plate.

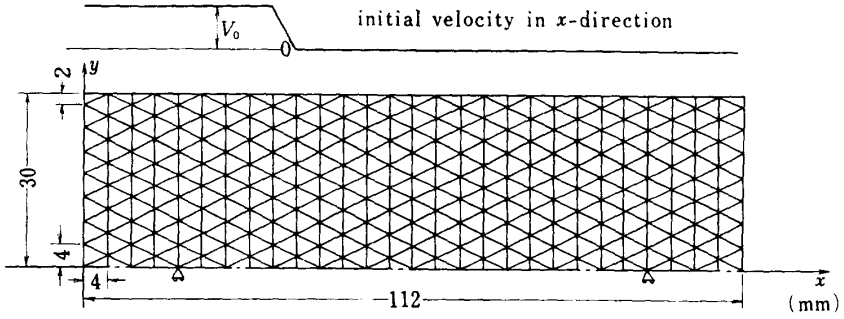

FIG. 3-7. The analyzed model of the stress wave in a strip, the model was divided into 448 elements by 261 points.

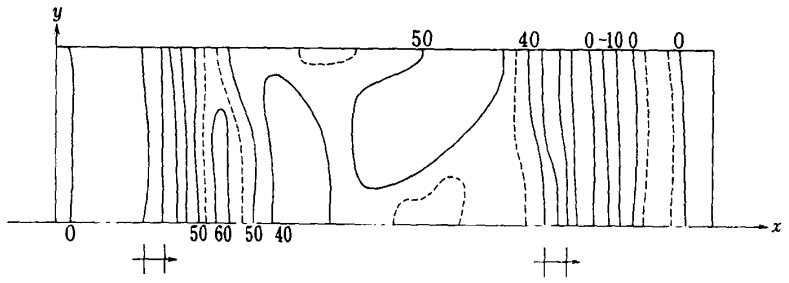

FIG. 3-8. The numerical result of the stress wave propagation in a strip. The principal stress distribution is shown. H denote the regioe of wave front.

This document is provided by JAXA.

In practice, we solved the stress wave propagation in a strip using this method. The solved model is shown in Fig. 3-7, where the thickness of the plate is 1 mm, the width is 30 mm (one end of the strip is fixed in this model, and this model is equivalent to a strip with a 6 mm width), the length is 112 mm, and as material constants, $E=2.0\times10^4$ kg/mm, $\nu=1/3$, and $\rho=8\times10^{-10}$ kg-s^2/mm^4 are used for the Young's modulus, the Poisson's ratio, and the density respectively. Dividing this model into 448 elements by 261 nodal points, the stress wave propagation was observed numerically by giving the initial velocity -2.5×10^4 mm/sec in the x direction to the 81 nodal points which are to the left of A in this figure. Then calculations were performed under the condition of plane stress, so that the stress wave $\sigma_0=53.033$ kg/mm^2 approximately travels with the velocity $c=5.303\times10$ mm/sec in both directions from the boundary of the points which have initial velocity and those which do not (*e.g.* A and B). The result of the numerical calculation is shown in Fig. 3-8. The calculation was performed setting $\Delta t=9.43\times10^{-8}$ sec. (*e.g.* $c\Delta t=0.5$ mm), and the principal stress distribution at $t=4.714\times10^{-6}$ sec. is shown. The marks H denote the stress wave front generated at A or B. The stress wave travelling to the right shows that there exists negative stress in front of the wave front, but behind it, there exist stress coincident with the analytical expectation. These results show a similarity with the one-dimensional calculation (Figs. 3-3, 3-4). Next, we examined the stress wave which travels to the left and then is reflected at the left end. On the left side of the stress wave front, the stress level becomes zero, and on the right side of this wave front the stress level is partly a little higher. This is the effect of the reflection of the negative stress, and these results agree with the trend of the one-dimensional analysis, too. From the one-dimensional analysis these disturbances can be expected to become smaller by selecting $c\Delta t/l$ properly. But in the two dimensional problems there exist two types of waves (dilatational and distortional waves), which travel with different speeds. Moreover we can not cover arbitrary shapes by the same regular triangles and make the length of the lines connecting the neighboring nodal points equal. Thus the error due to these causes can not be avoided. These errors can not be avoided for problems like stress wave propagation because the length by which the physical quantities are transported in one step calculation can not agree with the length of the coordinate in space. As for the convergency of the solution according to $c\Delta t/l$ in stress wave problems, F. Kikuchi and Y. Ando (8) have conducted detailed investigation, so this aspect will not be discussed here.

3-2 *Analysis of dynamic stress concentration*

In this section, elastic stress concentrations in notched plates as induced by stress waves are solved numerically using the finite element method.

3-2-1 *The analyzed model*

The models are isotropic and homogeneous strips with uniform thickness and symmetrical notches on the both sides as in Fig. 3-9. The contours of

This document is provided by JAXA.

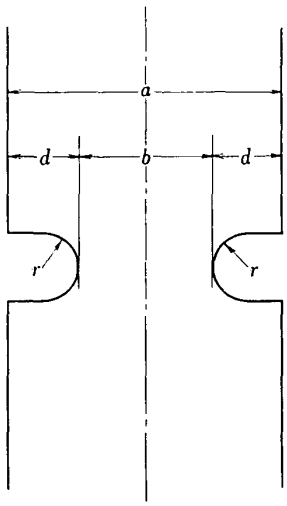

FIG. 3-9 The analyzed model.

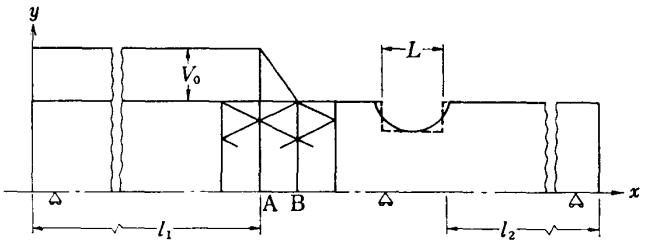

FIG. 3-10. The conditions of the analysis.

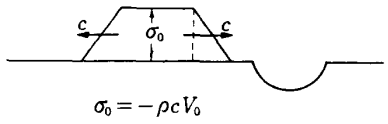

FIG. 3-11. The generated stress wave.

TABLE 3-1. The analyzed sets of a/b and r/d

a/b \ r/d	1/2	2/3	1	2/3	2	3
1.5		○	○	○	○	○
2	○	○	○	○	○	○
3	○	○	○	○	○	○
5	○	○	○	○		

the notches are given by circular arcs. Using a, b, r, and d as the width of the strip, the width of the narrowest section, the radius of curvature at the bottom of the notch, and the depth of the notch respectively, the calculations are carried out for various sets of a/b and r/d as shown in Table 3-1.

3-2-2 Numerical analysis using the finite element method

The numerical calculation was performed as follows. As the model is

This document is provided by JAXA.

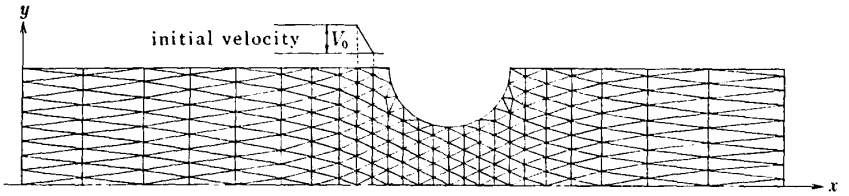

FIG. 3-12. An example of the devide into elements, $a/b=2$ and $r/d=1$. This case the continuum was divided into 377 elements by 225 nodal points.

symmetric with respect to the axis, the analysis is performed for about only half of the model as shown in Fig. 3-10. Taking the symmetrical axis as the x-axis, we restrict the displacement in the y-direction on the x-axis. To get the dynamic loading, initial velocity $-V_0$ is given in the x-direction for all the nodal points which exist at the left side of section A (Fig. 3-10). Then a stress wave of magnitude $\rho c V_0/2$ travels in both directions with the velocity c (Fig. 3-11). In this analysis l_1 and l_2 in Fig. 3-10 are so selected as to be $l_1=2.5\sim3L$ and $l_2=2\sim2.5L$, so that the stress is elevated 4~5 times by the reflections at the notch ends. But by the existence of disturbance in front of the wave front, we can not observe it for a long time. The time increment Δt by one-step calculation is selected as about one-forth of the time for the longitudinal wave to travel the shortest length between the nodal points. The models are divided into 300~400 elements by 200~250 nodal points, and the calculation is carried out for about 200 ~400 steps. In this calculation, 1/3 is used for the Poisson's ratio, and plane stress is assumed.

For instance, the scheme of the model $a/b=2$ and $r/d=1$ divided into elements is given in Fig. 3-12. The initial velocity is given for the nodal points to the left of A in this figure, and the distribution of σ_1/σ_0 and τ_{12}/τ_0 are shown in Figs. 3-13, where σ_1 and τ_{12} are the principal stress and the difference of the principal stresses respectively, and σ_0 and τ_0 are the values of those for the case of a uniform strip. In this figure the marks H denote the wave front generated from the borders of the initial velocity zero and V_0. The figures show that in the vicinity of the wave front stress arises as expected. The point of maximum stress is at first at the left side of the notch and then moves to the bottom of the notch. The principal stress difference is concentrated in the domain extending from the bottom of the notch and parallel to the symmetrical axis on the left side of the notch, and this is the largest point different from the maximum principal stress distribution. The stress distribution in the neighbourhood of the notch becomes very similar to that which is expected for the statical case even just after the stress wave has passed the notch. This shows the possibility of using the statical stress concentration factor as the first factor causing the dynamic stress concentration stated in section 2-3.

3-3 Comparison with the one-dimensional approximate solution

In this section, the numerical results by the finite element method are

This document is provided by JAXA.

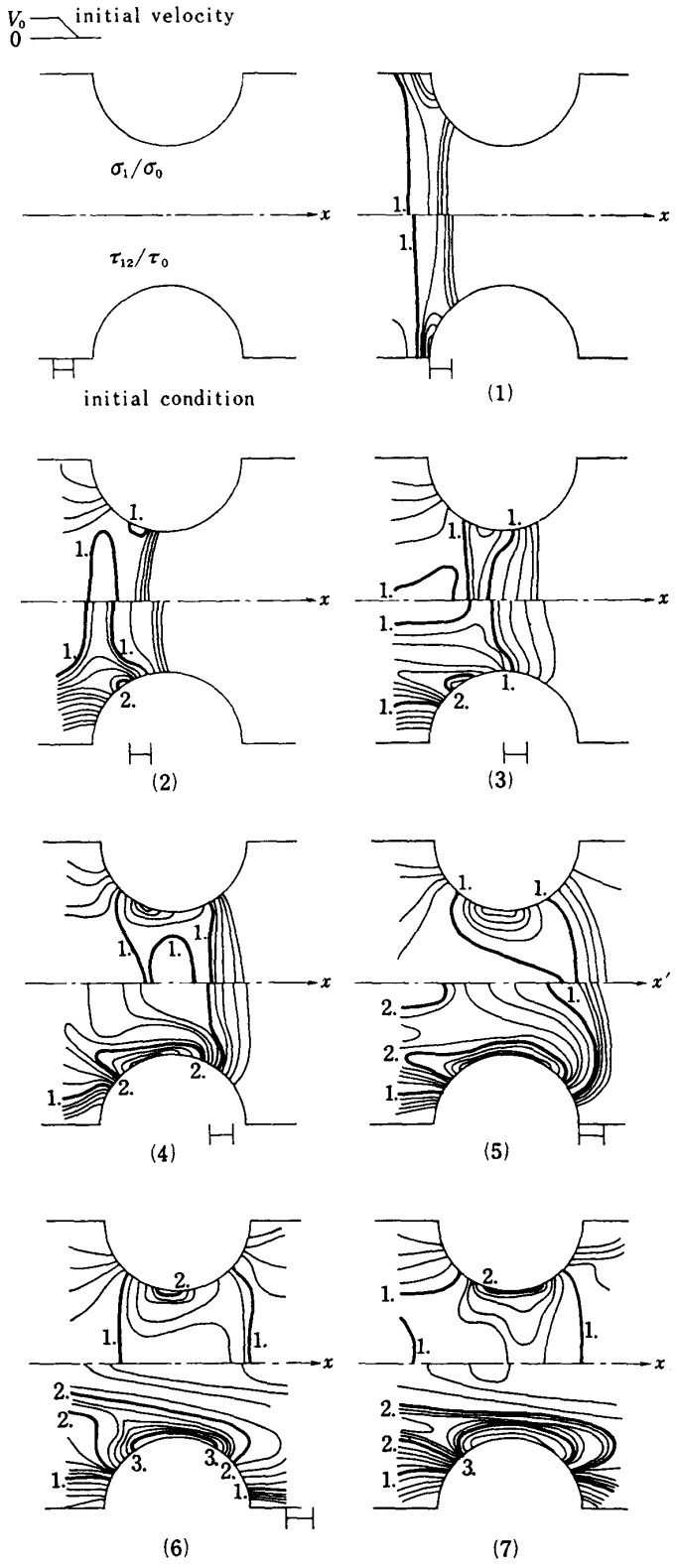

FIG. 3-13. Some schemes of the stress field. The principal stress and principal stress difference are shown. (Initial Condition) (1) (2) (3) (4) (5) (6) (7)

This document is provided by JAXA.

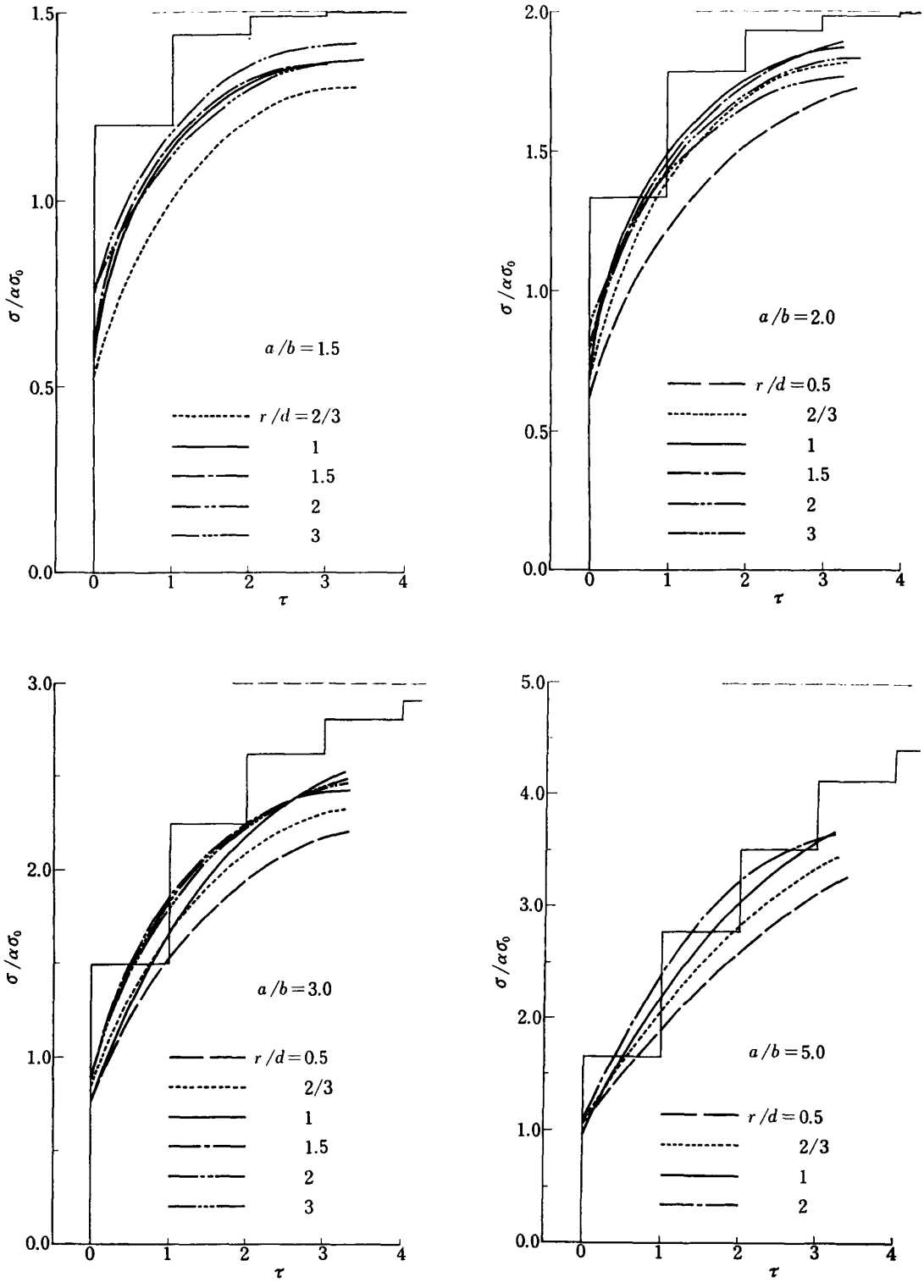

FIG. 3-14. The results of the dynamic stress concentration. The step line denote the one dimensional approximate solution, Eq. (2-32).

This document is provided by JAXA.

shown and compared with the one-dimensional approximate solution, Eq. (2-32), where α is the stress concentration factor, and σ_1 is the function given by Eq. (2-30). In Figs. (3-14), calculated $\sigma/\alpha\sigma_1$ are shown with the approximate solution Eq. (2-32). In these figures τ is $(t-t_0)c/L$, where t_0 is time when the stress wave front reaches the narrowest cross section, and σ_0 is the magnitude of incident stress wave. The statical stress concentration factors α in this figures are those calculated by the finite element method using the same divided models as used for dynamic analyses.

The two dimensional numerical calculation gives a little lower value than the approximate solution given by Eqs. (2-32) and (2-30-b), especially when r/d is small, that is, when the radius of the notch bottom is small compared with the depth of the notch. But when r/d is large, this gives close agreement. Perhaps this can be attributed to the fact that when the depth is shallow compared with the radius of the notch bottom, the stress wave behaves more like a one-dimensional model. In conclusion, the approximate solution given by Eqs. (2-32) and (2-30-b) is good enough for industrial use.

§ 4 Experimental Analysis Using High-speed Photoelasticity

In the present section the instrument and the procedure of photoelasticity used for the analysis are explained first, and then the results of the experiment are shown and compared with the one-dimensional approximate solution.

4-1 The instrument used for the experiment of photoelasticity

The instrument used for this experiment is a spark gap camera (High-Speed 16 Frame Multiple Spark Gap Camera (Materials Research Lab. Inc., MRL-MGHSPS-16-04-CXIII, Fig. 4-1)). This camera is composed of three basic subsystems which include a pulsing spark-gap assembly, an optical system, and a synchronization circuit. Each of these subsystems is described individually in detail in the following subsections.

4-1-1 The pulsing spark gap assembly

A square array (4×4) of 16 spark gaps provides a time sequenced series of short-duration high-intensity light flashes used both to illuminate the

Fig. 4-1. The Spark Gap Camera used for the experiment.

This document is provided by JAXA.

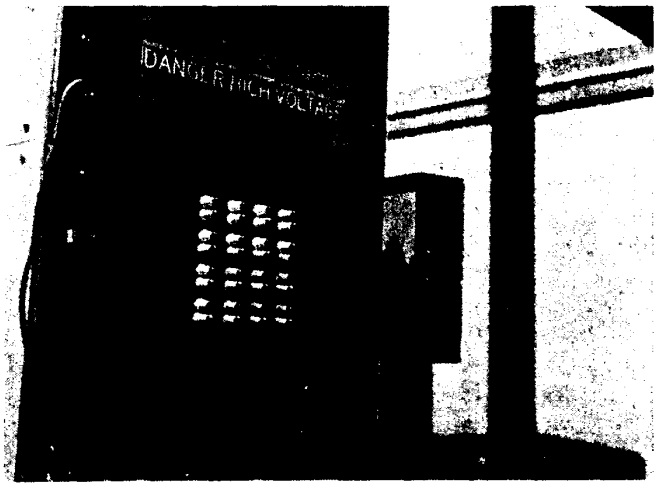

FIG. 4-2. Spark Gap Assembly (4×4 Array).

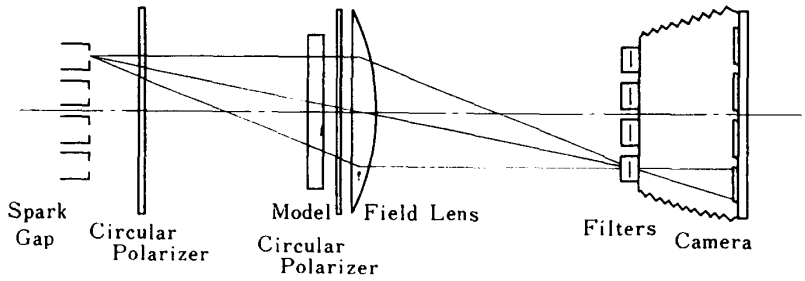

FIG. 4-3. Arrangement of the Optical System.

object and to shutter the camera. As shown in Fig. 4-2, each gap consists of two 0.500 in. diameter bronze spheres positioned 0.750 in. on center to give fixed gap length of 0.250 in.. The square 4×4 array of gaps is arranged on 2 in. centers. The array of spark gaps is energized by a series connected L-C type pulse circuit, and the time intervals are controlled from 1.13 μsec. to 33.30 μsec. by varying the connection of the circuit, and 11 selections are possible.

4-1-2 Optical system

The optical system associated with the camera performs three distinct functions which include image separation, recording the image, and producing circularly polarized light which is nearly monochromatic. A schematic illustration of the complete optical system is showh in Fig. 4-3. The light emerging from a given spark gap passes through a model in a standard light field polariscope and is collected by a large diameter field lens. The field lens then focuses the light on a single camera lens where it in turn passes through a filter and focuses on a film plane.

Image separation, that is the independent recording of 16 separate negatives of the dynamic event, is accomplished by the geometric spacing of the spark gap and the position of the field lens. For the optical arrangement used with this system, the spark gaps and the camera lenses are both placed on a 4×4 square array on two inch centers. Using 16 matched Kodak Ana-

This document is provided by JAXA.

stimate camera lenses, each with a focal length of 161 mm, f 4.5, enables the recording of 16 distinct and separate images in a controlled time sequence.

The magnification of the optical system is essentially fixed as it is controlled primarily by the focal lengths of the field and camera lenses, and their relative spacing. With this system a magnification ratio of about 0.11 is obtained to give an image diameter of 2 inches corresponding to the 18 inch diameter field lens. The 4×4 array of 16 images, etch 2 inches in diameter, is recorded on a single sheet of 11×14 in. film mounted in a conventional view camera.

The film employed in recording the images is Kodak Gravure Positive. This film is sensitive to light between 3500 and 5100 Å and it is employed with Kodak Wratten filters no. 8 which cut off most of the light below 4800 A. These filters are mounted on a plexiglass plate located in the commercial view camera directly behind the lens board. This combination of film and filters yields a transmitted and recorded band width from 4800 to 5100 Å which is sufficiently narrow (300 Å) to approximate monochromatic light in dynamic photoelastic applications.

A simple yet effective dynamic polariscope is incorporated into the optical system by placing two sheets of Polaroid HNCP-38 (plastic-laminated circular polaroid) between the field lens and the spark gaps. The forward sheet of polaroid is mounted on the front of the protective box which encloses the spark gaps. The aft sheet of Polaroid is mounted behind the glass plate which protects the field lens.

4-1-3 Synchronization Circuits

In the dynamic photoelastic application to the problem under consideration, the time of the event ranges from about 100 to about 200 μsec.. In this brief interval the model must be loaded, the camera delayed and then initiated, and the time of the individual frames recorded. The necessary control is accomplished by the synchronization circuit shown schematically in Fig. 4-4. The sequence of events is initiated by dropping the specimen on a block of steel. Then the stress wave arising in the block is picked up by an electro-acounstic transducer (Piezotite, Murata MFG. Co. Ltd.) which is set near the falling point. By the signal from the transducer the trigger circuit is closed, and the time delay generator is activated.

After a preselected delay time, the delay generator transmits a pulse to

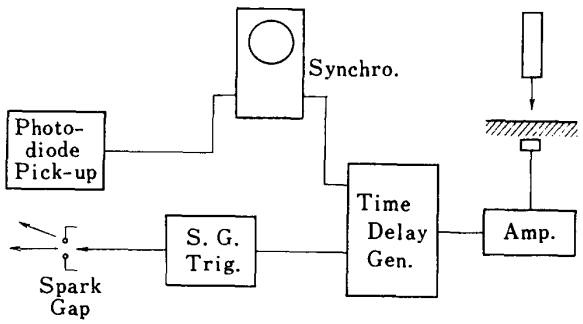

FIG. 4-4. Schematic of Synchronization circuit.

This document is provided by JAXA.

the trigger module. This trigger module acts as a pulse amplifier, and after a few microseconds delay time, it issues a high voltage output pulse. This high voltage pulse is applied to the third electrode of the trigger gap causing it to conduct and to initiate the firing sequence in the bank of spark gaps.

As the spark gaps are sequentially fired the light intensity is monitored as a function to time with a high speed photodiode. The out put of the photodiode is recorded on a sweeping oscilloscope to give an intensity time profile. This profile has 16 distinct peaks and gives the precise time during the dynamic event when each of the 16 frames is recorded.

4-2 Experiment Procedure

Adequately recording the dynamic event requires that a large number of operations be performed in proper sequence with a high degree of precision. As the dynamic event is only for a few hundred micro seconds there is no time for a second chance or a minor adjustment, and this fact necessitates the careful preparation of the experiment. The description of the operating procedure is as follows :

1) The optical system is aligned by placing a small high intensity lamp in the gap of the spark gap at one corner and by adjusting the camera front so that a circle of light falls on the center of the lens cap for the corresponding lens. This procedure is repeated for the four conrner gaps to simultaneously obtain the alignment of all four corner gaps and lenses. If the alignment of the optical system is not obtained adequately, the images on the film will be distorted.

2) The set-up model is in its proper location in Fig. 4-5.

3) Using the high intensity lamp and a focusing negative the camera back is adjusted (without moving the camera front) to bring the model into focus.

4) The delay generator is adjusted for the initial delay period, and proper time intervals for the sparks of the spark gaps are selected.

5) Power is supplied to the spark gaps.

FIG. 4-5. The specimen put in position.

This document is provided by JAXA.

6) The film holder is placed in the camera and the film slide is pulled out.

7) The specimen is dropped.

8) The film slide is closed.

9) All switches are turned off.

By this procedure the photogragh of photoelasticity is obtained and the sequence of the light is recorded by the Polaroid camera set on the oscilloscope.

4-3 Experimental results and comparison with the approximate solution

The photoelastic experiment was carried out using epoxy specimens shown in Fig. 4-6. All the specimens had semicircular notches with diffenent radii and the material constants are shown in Tabl. 4-1. Dynamic compression was applied to the specimens by dropping the specimens on a block of steel. The bottoms of the specimens were tapered so as to be able to get uniform compression. The time intervals of the photographs were 6.57 μsec., 6.57 μsec., 8.40 μsec. and 12.3 μsec. for specimens $a/b=1.5$, 2, 3 and 5 respecti-

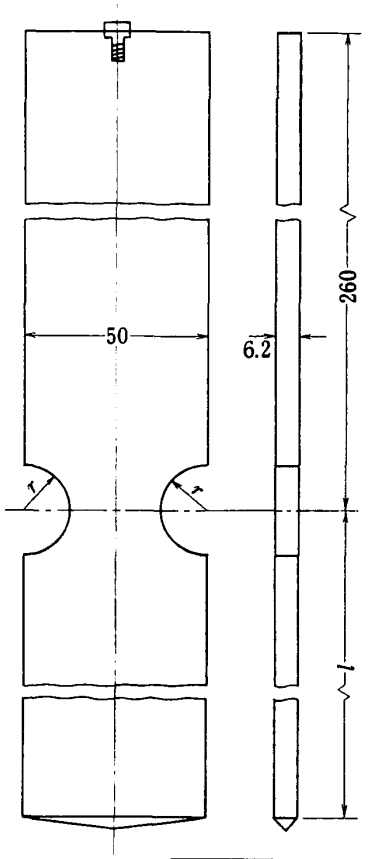

a/b	r	l
1.5	8.3	180
2	12.5	180
3	16.7	190
5	20.0	230

FIG. 4-6. The photoelastic model.

This document is provided by JAXA.

TABLE 4-1. The material properties of the epoxy specimens.

ρ	1.22×10^{-10} kg·s²/mm⁴
E	321 kg/mm²
ν	0.375

vely. The photographs of isochromatics are shown in Figs. 4-7, 4-8, 4-9 and 4-10. They show that the wave fronts do not rise discontinuously but continuously. The time necessary for the stress to rise to uniform stress is long enough for the stress wave to travel the length of the notch, so that the rising time of the stress must be considered for the analyses of the experimental results.

From the fringe order points of 0.5 and 1.5 in the photographs before the wave front reaches the notch, the shape of the incident stress wave is approximated as shown in Fig. 4-11, and the length 1 and the fringe orders at the uniform stress field become as shown in Tabl. 4-2. The equivalent notch length L and the statical stress concentration factor α given by Eq. (2-31) are also shown in Table. 4-2. Using these values and reading the fringe orders at the bottom of the notch, the values σ/σ_∞ are plotted in Fig. 4-12, where σ_∞ is the stress to which the one-dimensional approximate solution tends when t increases infinitely. Simultaneously the approximate solution given by Eq. (2-36) and the two dimensional numerical solution are shown in this figure, where the numerical solution is obtained by substituting the values read from Figs. (3-14) into Eq. (2-36).

These results show that the one-dimensional approximate solution gives very close agreement with two dimensional numerical solutions and experiments, and gives slightly greater values than them. They give close agreement, especially when the notch is wide compared with the radius of the notch bottom, but when the notch becomes deep the approximate solution tends to give a large value. These can be attributed to the fact that when the notch becomes deeper the difference with the one dimensional hypothesis becomes greater. The experimental results give smaller values than numerical

TABLE 4-2. The shapes of the incident stress waves.
l: the necessary length that the incident stress wave reaches a uniform stress level.
L: the equivalent length of the notch.
n_0: fringe orders at the uniform stress field.
α: stress concentration factor.

a/b	l (mm)	L (mm)	l/L	n_0	α
1.5	84.2	14.4	5.83	1.8	1.98
2	97.4	21.7	4.50	1.8	1.64
3	89.2	28.9	3.09	2.8	1.37
5	90.6	34.6	2.62	2.0	1.19

This document is provided by JAXA.

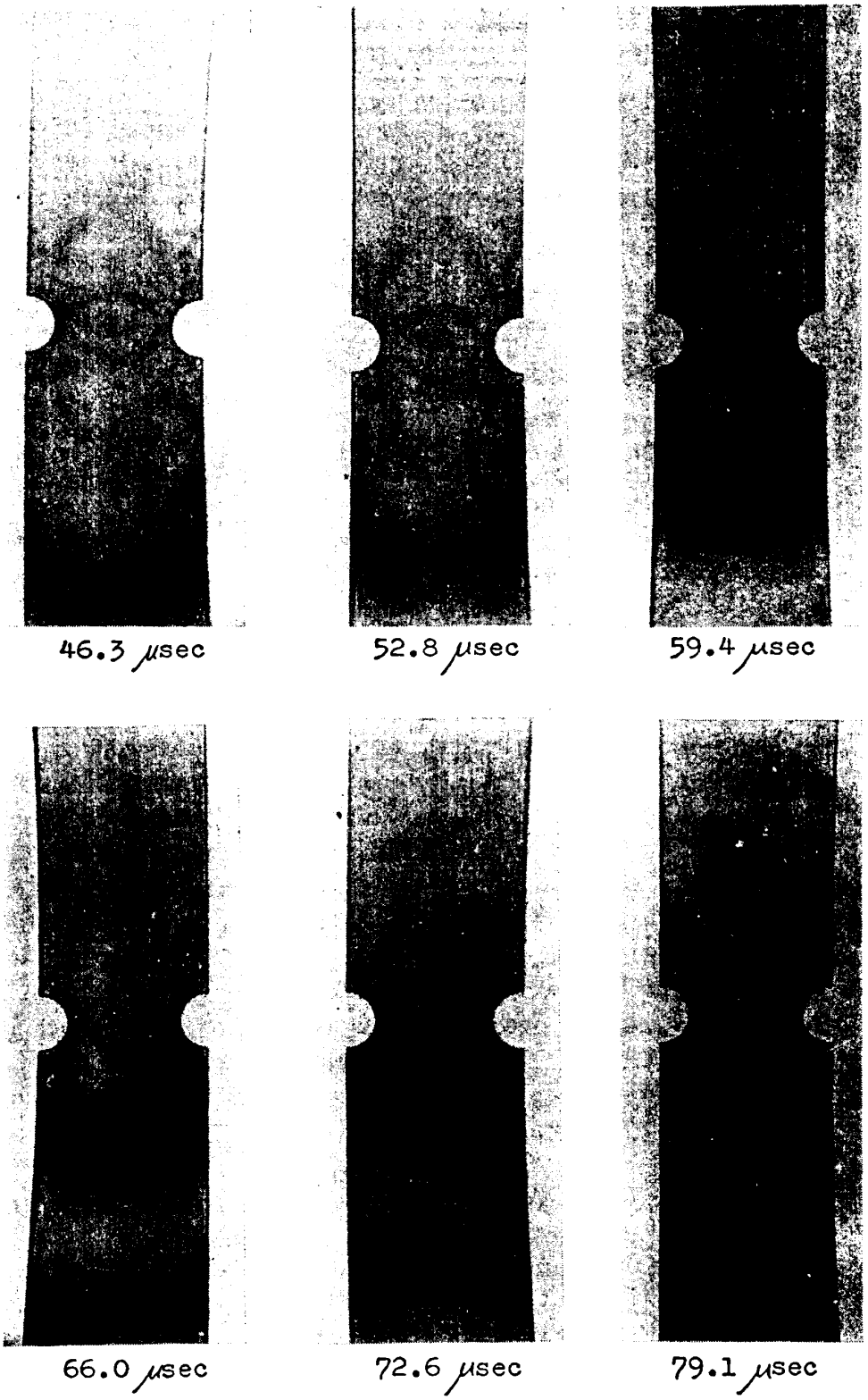

FIG. 4–7. Photoelastic stress patterns for $a/b=1.5$.

This document is provided by JAXA.

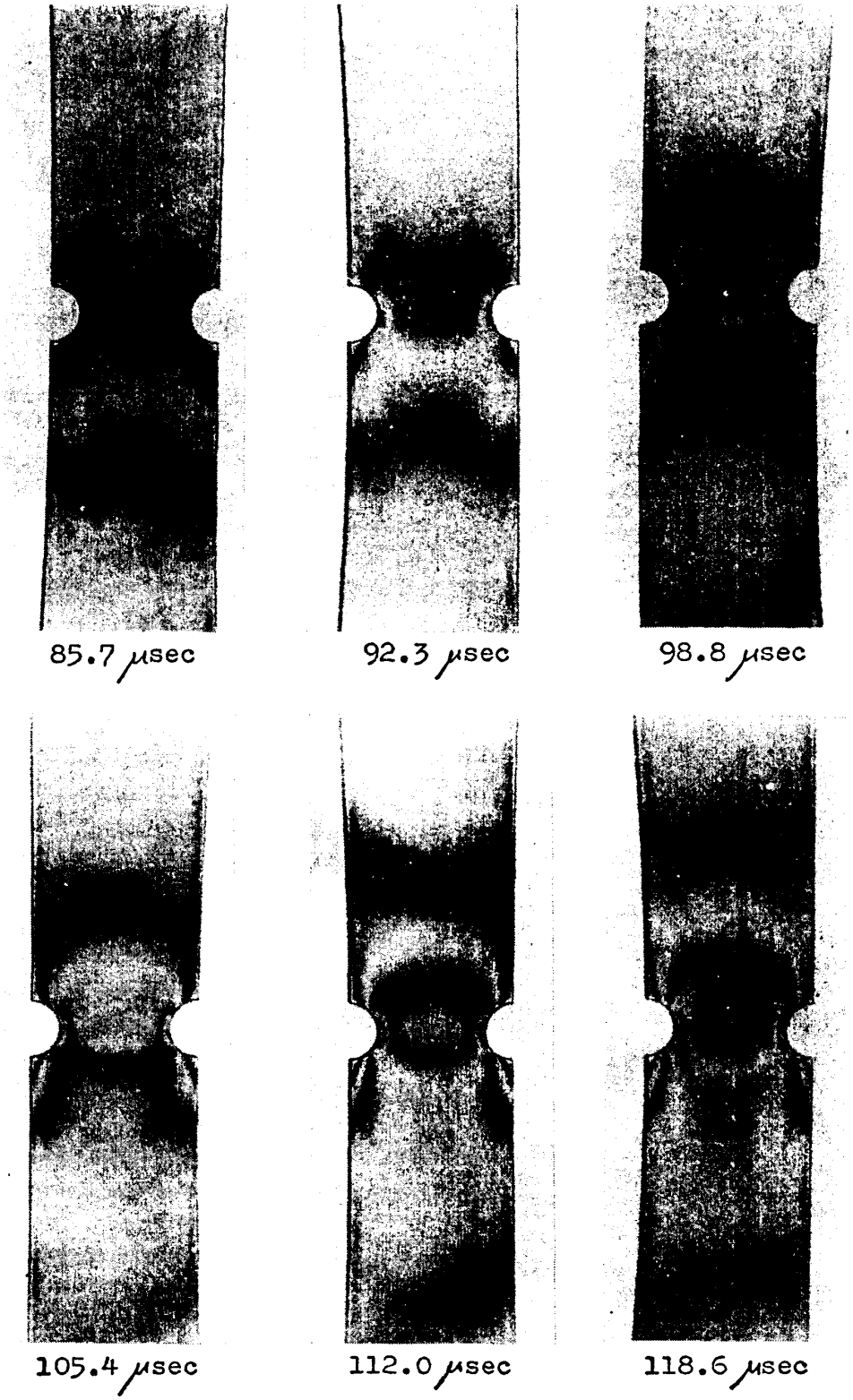

FIG. 4-7. (Continued.)

This document is provided by JAXA.

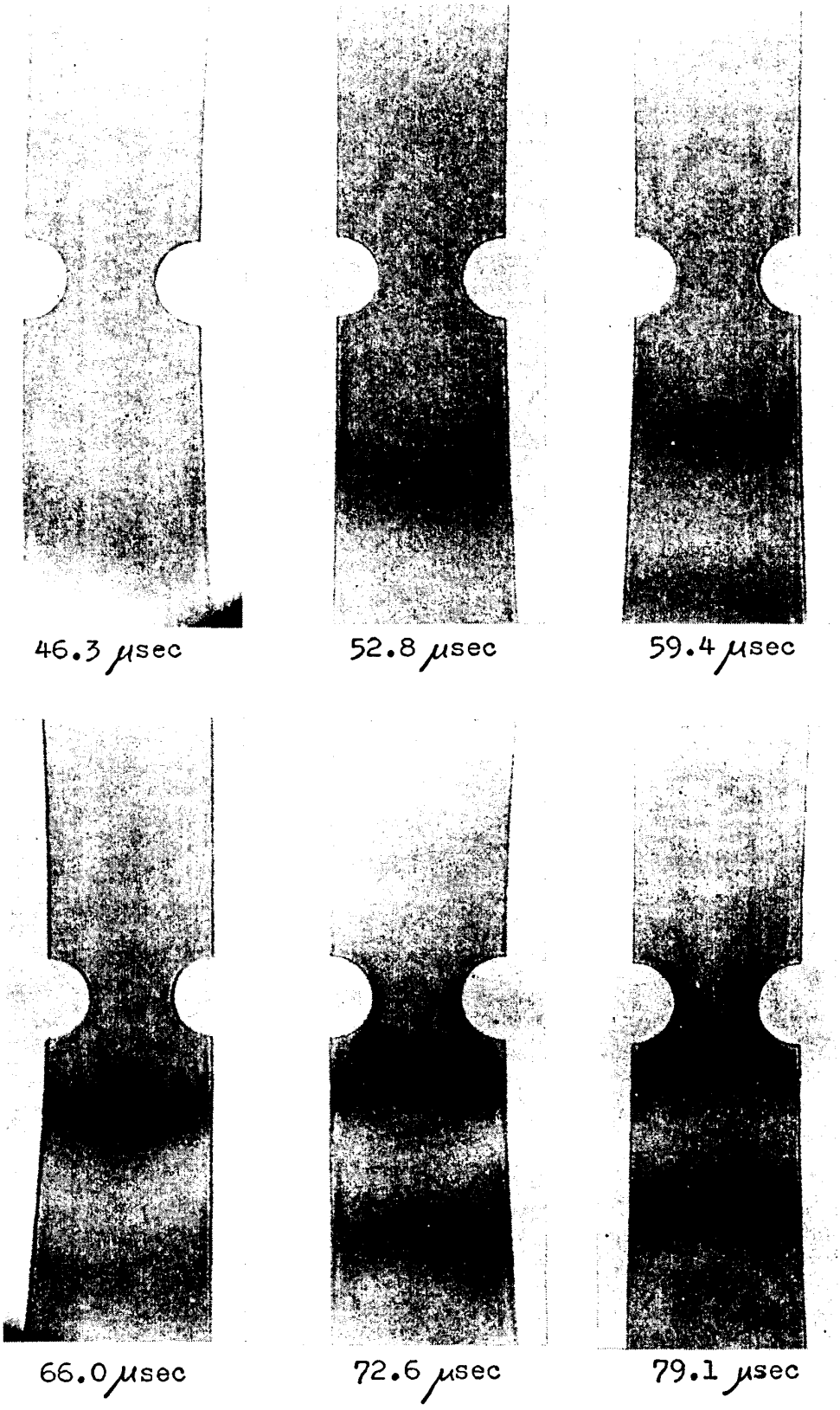

FIG. 4–8. Photoelastic stress patterns for $a/b=2$.

This document is provided by JAXA.

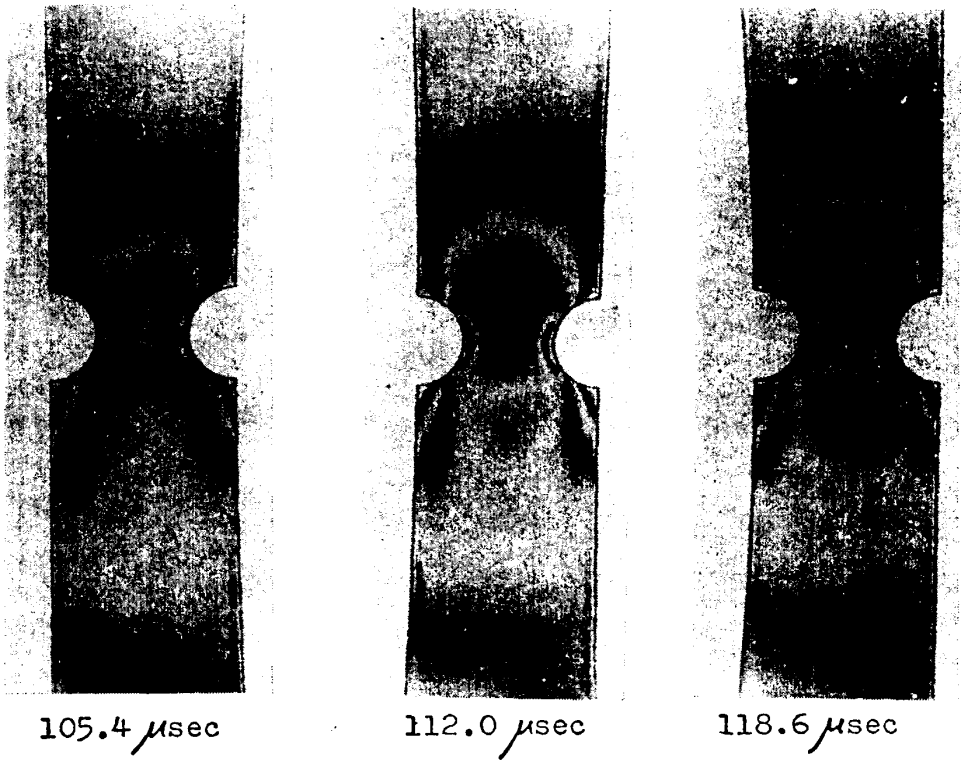

FIG. 4-8. (Continued.)

This document is provided by JAXA.

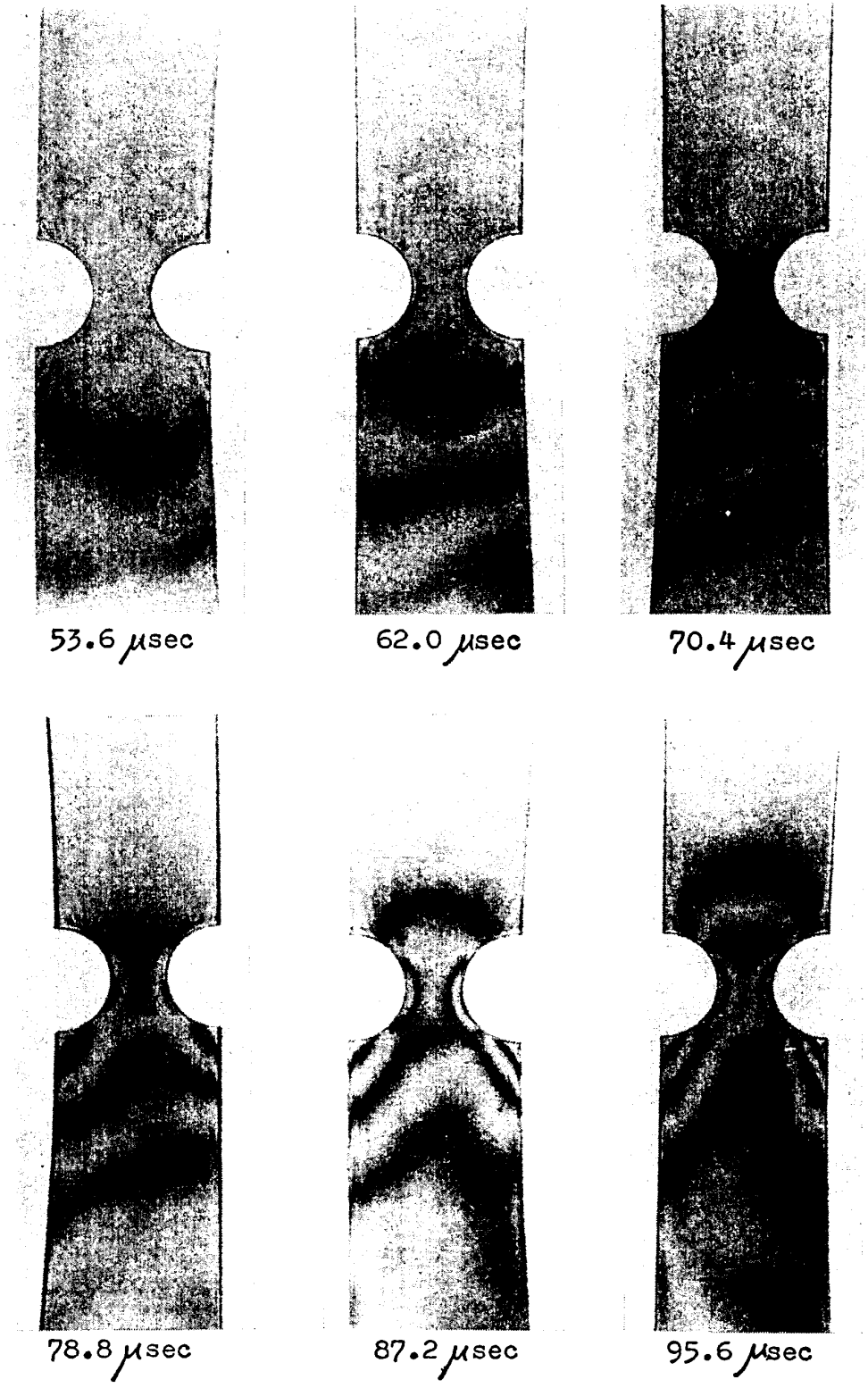

FIG. 4-9. Photoelastic stress patterns for $a/b=3$.

This document is provided by JAXA.

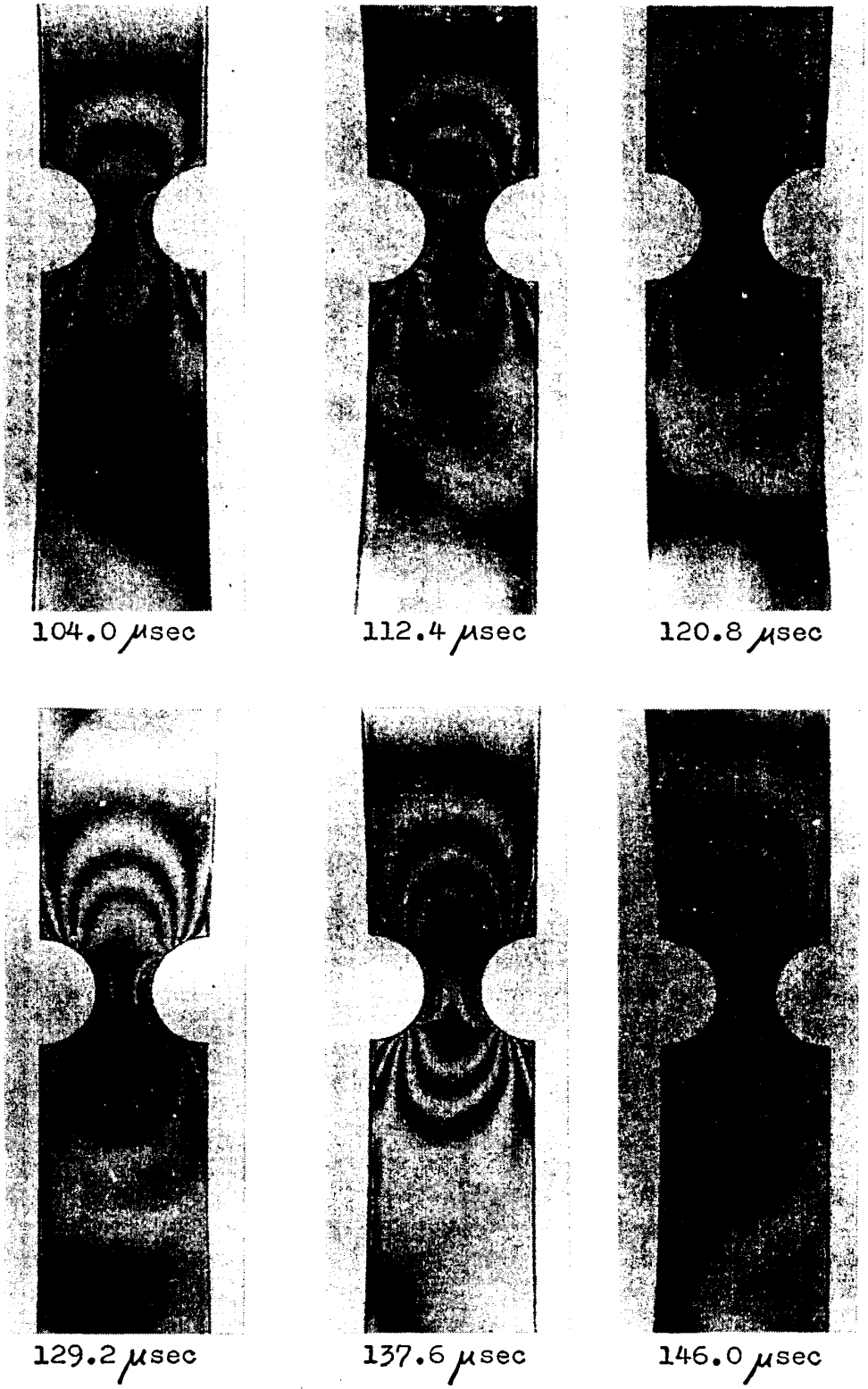

FIG. 4–9. (Continued.)

This document is provided by JAXA.

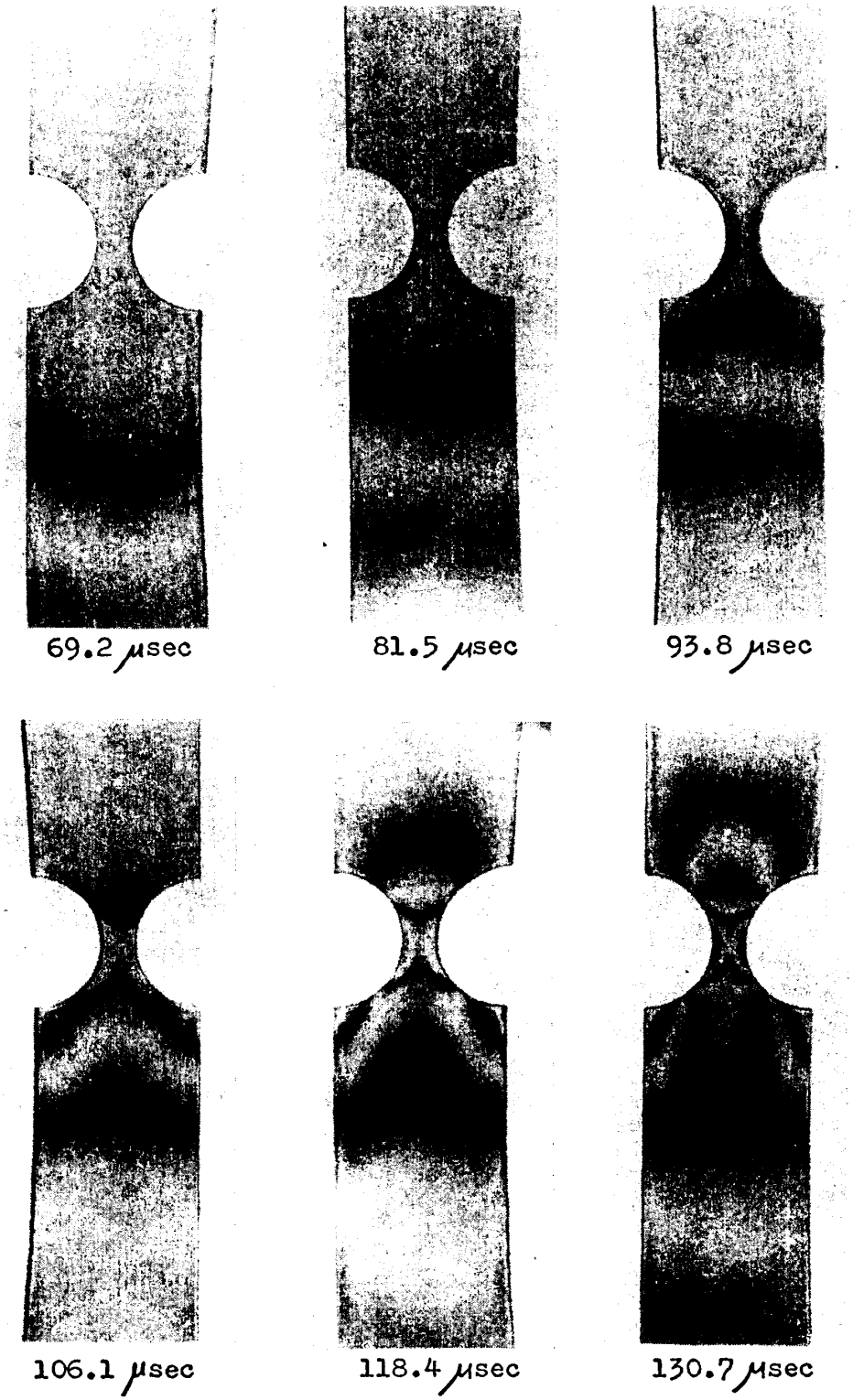

FIG. 4-10. Photoelastic stress patterns for $a/b=5$.

This document is provided by JAXA.

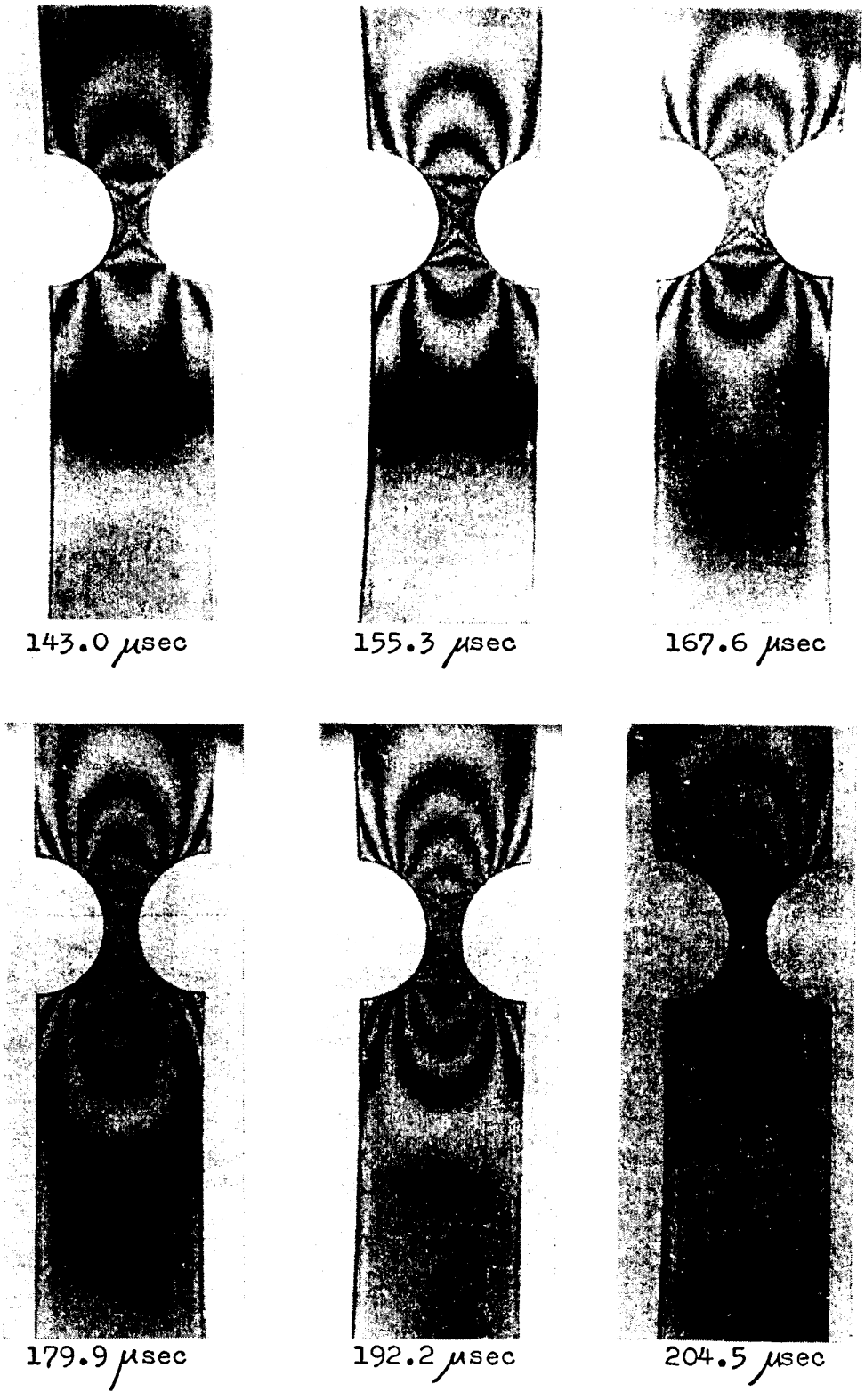

FIG. 4-10. (Continued.)

This document is provided by JAXA.

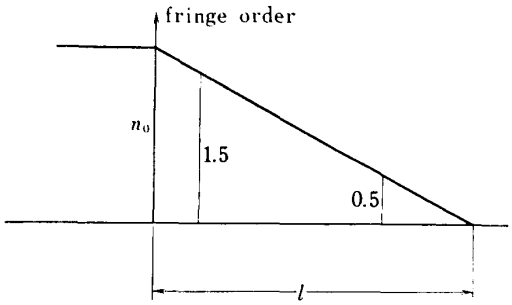

FIG. 4-11. The approximation of the stress field arising near the wave front.

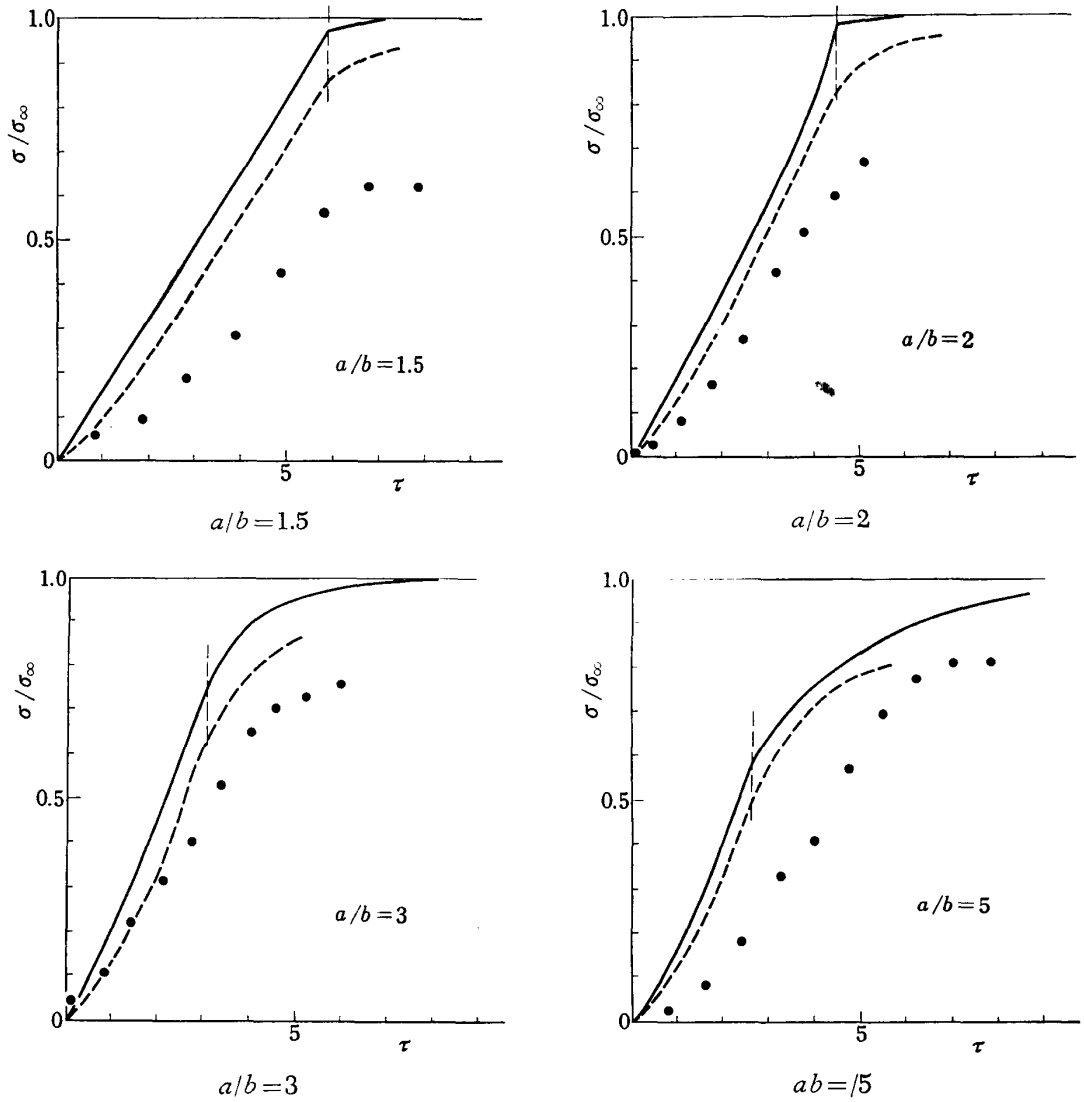

FIG. 4-12. The stress concentration at the bottom of the notch. The experimental results are compared with the approximate solution and two dimensional numerical results.

——; the one dimensional approximate solution
----; two dimensional numerical results
· ; the experimental results

This document is provided by JAXA.

results, which may be caused by the fact that the specimens are too small to read the fringe orders accurately enough.

In conclusion, the one dimensional approximate solution can be considered to give close agreement with two dimensional numerical results and experimental results, especially when the notch becomes shallower when compared with the radius of the notch bottom. Then approximate solution is also useful enough for engineering designs.

§ 5 Conclusion and Discussion

In this report the elastic stress concentrations of notched plates as induced by tensile stress wave were examined. First, this problem was analysed using the one-dimensional theory of stress wave propagation, and an approximate solution was obtained. Then this problem was analysed numerically using the finite element method and experimentally using high-speed photoelasticity, and these results were compared with the one-dimensional approximate solution to confirm the effectiveness of this approximate solution.

Hereafter the points made clear in this report are shown for each chapter.

In § 1 the significance and the historical view of the problem of elastic stress concentrations in notched plates as induced by stress waves were represented, and the outline of this report was stated.

In § 2 the one-dimensional theory of stress wave propagation was explained, and then using this theory an approximate solution of elastic stress concentration was obtained. In this solution, the dynamic stress conceration was considered to consist of two factors, the first was the result of the stress gradient in the narrowest cross section and the second was the result of the differences of the cross-sectional areas. For the first factor the statical stress concentration factor α, and for the second factor the one-dimensional theory of stress wave propagation were used. The approximate solution was represented as the product of two factors,

$$\sigma = \alpha \sigma_1.$$

At first, the solution was obtained for the case when the incident stress wave was given by a step function, then the solution was extended to the case of an arbitrary shape incident wave.

In § 3 the application of the finite element method to dynamic problems was presented, and then using this method the stress wave propagation in a rod was solved one-dimensionally and in a strip two-dimentionally. These results were then compared with the analytical result, and the effectiveness and the limitations of the application of the finite element method to dynamic problems were examined. Next, the elastic stress concentrations of notched plates as induced by waves were computed numerically using this method and then compared with the one-dimensional approximate solution. The two dimensional numerical solutions were a little lower than the approximate solution. The differences of both results became large especially when the notch was deep relative to the width of the notch and the radius of curvature

This document is provided by JAXA.

of the notch bottom. When the notch is much deeper compared with the width, then the behaviour of the stress waves becomes different from the one-dimensional hypothesis, and some other treatment is required for these cases. But for the case of wide and shallow notches the above two results indicated close agreement, and the approximate solution is considered useful for the engineering designs.

In § 4 the instrument used for the photoelastic experiments, the spark gap camera, and the experimental procedure were explained. Then the dynamic elastic stress concentrations of notched plate were observed using epoxy specimens with semi-circular notches, and the results were compared with the one-dimensional approximate solution and two dimensional numerical results. The experimental results were in general, in close agreement with the other analyses, but gave numerically slightly lower values, especially when the notches were shallow compared with widths of the strips. This can be explained by the fact that it is very difficult to read the fringe orders at the bottom of the notch precisely when the notch becomes small, and some errors did appear in reading the fringe orders. But when the notch was large, the experimental results showed close agreement with the theoretical analyses.

From these results we can conclude that the approximate solution is useful for engineering designs except for the case when the notch is deep and narrow.

In the process of this investigation some problems emerged for the future investigation.

1) In the analysis of the finite element method, there emerged some disturbances in front of the wave front. This phenomenon occurred because the distances of the neighbouring nodal points were different from the length that the physical quantities travel in one step calculation. By adequate selection of the time increase in one step calculation or by the adequate division into elements, this error is expected to become smaller. Using fundamentally different types of elements, *e. g.* hexagonal elements with six nodal points, where the stresses and strains are permitted to vary in one element, the accuracy of the analyses may become higher, sovinvestigation of this point is necessary. In particular the authors consider that the above mentioned should be taken into consideration when analyzing the problems of the dynamic plasticity using this method.

2) When the notch becomes narrow and deep, or has a crack, some other treatment is necessary. To investigate the stress field around a crack is very important and necessary theme for future study.

3) Until the present, two or three dimensional analysis of stress wave propagation has not been conducted so much because of the difficulty to solve the wave equations, and the solved examples have been confined to problems with simple boundaries. However complex boundary problems have become possible to solve numerically using the finite element method. Henceforth we need to solve practical problems and clarify the dynamic responses of materials and structures, not only elastically but also plastically.

This document is provided by JAXA.

Acknowledgment

The authors wish to express their appreciation to professors M. Sunakawa, D. Mori and A. Kobayashi of this institute, and to professors S. Kobayashi and J. Shioiri of the University of Tokyo for the helpful suggestions and discussions. The authors also thank to Mr. S. Hashimoto for his help in experiments.

Department of Material
Institute of Space and Aeronautical Science
University of Tokyo
March 20, 1976

References

[1] K. Kawata and S. Hashimoto; "On Some Analyses of Dynamic Stress Concentration due to an Elastic Wave with a Long Plateau of Constant Stress", Bulletin of the Institute of Space and Aeronautical Science, University of Tokyo, Vol. 1, No. 2 (April 1965), 69–102 (in Japanese).

[2] K. Kawata and S. Hashimoto; "On Photoelastic and Theoretical Analyses of Some Dynamic Stress Concentrations by Elastic Waves", JSME 1967 Semi-International Sympo. -Papers, Exp. Mech., 1 (1967, Tokyo), 111–118.

[3] K. Kawata and S. Hashimoto; "On the Dynamic Stress Concentration in an Long Elastic Bar with Notches under Dynamic Tension", Bulletin of the Institute of Space and Aeronautical Sciencs, University of Tokyo, Vol. 8, No. 2 (B) (June, 1972), 377–384 (in Japanese).

[4] H. Kolsky; "Stress Waves in Solids", Dover Reprint (1953).

[5] M. Nisida; "Stress Concentration", Morikita Shuppan (1967) (in Japanese).

[6] J. S. Przemieniecki; "Theory of Matrix Structural Analysis", McGraw-Hill (1968).

[7] O. C. Zienkiewicz; "The Finite Element Method in Enginering Science", McGraw-Hill (1971).

[8] F. Kikuchi and Y. Ando; "A Finite Element Method for Initial Value Problems", Proc. Method Conf. on Matrix Methods in Structural Mechanics, (1971, Ohio), 169–213.

This document is provided by JAXA.